PALEOCEANOGRAPHY, VOL. 14, NO. 3, PAGES 273-292, JUNE 1999

Miocene evolution of atmospheric carbon dioxide

Mark Pagani,[1] Michael A. Arthur, and Katherine H. Freeman

Department of Geosciences, The Pennsylvania State University, University Park

Abstract. Changes in pCO_2 or ocean circulation are generally invoked to explain warm early Miocene climates and a rapid East Antarctic ice sheet (EAIS) expansion in the middle Miocene. This study reconstructs late Oligocene to late Miocene pCO_2 from ε_p values based on carbon isotopic analyses of diunsaturated alkenones and planktonic foraminifera from Deep Sea Drilling Project sites 588 and 608 and Ocean Drilling Program site 730. Our results indicate that highest pCO_2 occurred during the latest Oligocene (~350 ppmv) but decreased rapidly at ~25 Ma. The early and middle Miocene was characterized by low pCO_2 (260-190 ppmv). Lower intervals of pCO_2 correspond to inferred organic carbon burial events and glacial episodes with the lowest concentrations occurring during the middle Miocene. There is no evidence for either high pCO_2 during the late early Miocene climatic optimum or a sharp pCO_2 decrease associated with EAIS growth. Paradoxically, pCO_2 increased following EAIS growth and obtained preindustrial levels by ~10 Ma. Although we emphasize an oceanographic control on Miocene climate, low pCO_2 could have primed the climate system to respond sensitively to changes in heat and vapor transport.

1. Introduction

Long-term climate trends of the Cenozoic, inferred from detailed benthic foraminiferal $\delta^{18}O$ records, exhibit a pattern of high-latitude cooling and increased ice volume since the early Eocene [*Miller et al.*, 1987]. Importantly, global climates did not change steadily through time. Rather, oxygen isotope records record rapid, "step-like" cooling episodes at the base of the Oligocene, the middle Miocene, and the middle Pliocene [*Miller et al.*, 1987], which account for a significant proportion of overall change during the Cenozoic. These cooling events could represent climatic adjustments triggered when critical threshold levels of one or more parameters of the climate system were breached [*Kennett*, 1977; *Crowley and North*, 1988; *Zachos et al.*, 1993]. However, there is no consensus concerning the parameter(s) responsible for short-term (kyr) or long-term (m.y.) -scale climate change. Discussion generally centers on two controlling factors: (1) alterations in ocean circulation driven by tectonically induced changes in basinal topography [*Kennett*, 1977; *Woodruff and Savin*, 1989; *Wright et al.*, 1992] and (2) variation in carbon dioxide concentrations [*Vincent and Berger*, 1985; *Raymo*, 1991]. Although these processes are often considered independently, the role they played in creating climate change may not be mutually exclusive.

This study evaluates the importance of pCO_2 variability as an agent of climate change during the early to late Miocene. Specifically, we develop pCO_2 estimates on the basis of isotopic compositions of individual organic compounds derived from haptophyte algae and carbonates from surface-dwelling foraminifers.

[1]now at Earth Science Department, University of California, Santa Cruz.

Paper number 1999PA900006.
0883-8305/99/1999PA900006$12.00

1.1. Neogene Climate Change

Initially, researchers argued for minimal continental ice from sometime in the Cretaceous to the Miocene, with the transition to full "icehouse" conditions designated in the middle Miocene [*Shackleton and Kennett*, 1975; *Savin et al.*, 1975]. However, accumulative evidence now supports the development of large-scale glacial conditions in the early Oligocene, with the expansion and contraction of ice volumes throughout the Oligocene and early Miocene [*Miller et al.*, 1987; *Bartek et al.*, 1991; *Zachos et al.*, 1992, 1996, 1997; *Pekar and Miller, 1996; Miller and Sugarman*, 1995]. Trends in benthic foraminiferal $\delta^{18}O$ values provide evidence for at least nine glacial intervals during the Miocene, four of which occurred during the early Miocene [*Miller et al.*, 1991] (Figure 1). Nonetheless, a period of global warming followed a major glacial episode at the Oligocene/Miocene boundary [*Zachos et al.*, 1997], resulting in a reduced latitudinal temperature gradient and higher average surface water and deep water temperatures. At the height of the climatic optimum (~17 Ma), deep water and high-latitude surface water temperatures were as much as 6°C warmer than today [*Shackleton and Kennett*, 1975; *Savin et al.*, 1975]. Termination of this episode of relative global warmth was dramatic. A permanent $\delta^{18}O$ shift of ~+1‰ beginning at ~14.5 Ma (Figure 1) is interpreted to reflect rapid deep water cooling and East Antarctic ice sheet (EAIS) expansion [*Shackleton and Kennett*, 1975; *Savin*, 1977; *Miller et al.*, 1987; *Wright et al.*, 1992; *Flower and Kennett*, 1993]. High-latitude surface waters cooled while low-latitude water temperatures warmed [*Savin et al.*, 1985; *Flower and Kennett*, 1993], leading to a stronger latitudinal temperature gradient, increased vertical water mass stratification, and inferred strengthened surface water circulation [e.g., *Thunell and Belyea*, 1992].

1.2. Inferred pCO_2 Variability

Climate change hypotheses involving Neogene pCO_2 variability have been generated by inference from a variety of data including inorganic carbon $\delta^{13}C$ values [*Vincent and Berger*,

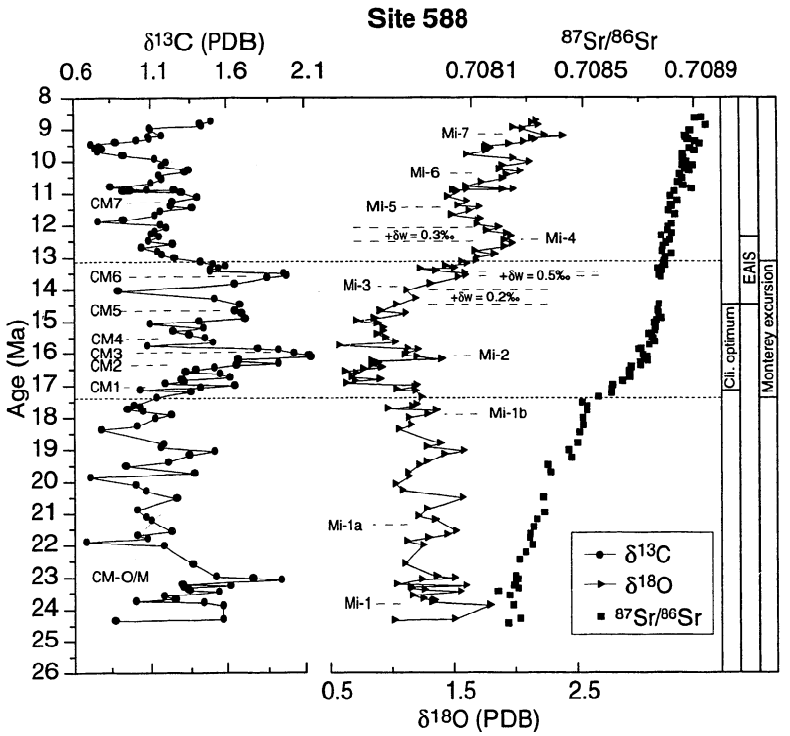

Figure 1. Isotope profiles from Deep Sea Drilling Project (DSDP) site 588. Solid circles and triangles represent $\delta^{13}C$ and $\delta^{18}O$ of benthic foraminifera, respectively. Data are from *Kennett* [1985]. Sr isotope ratios are represented by solid squares from [*Hodell et al.*, 1991]. Carbon maxima (CM) events (CM-Oligocene/Miocene (O/M), CM1-CM7) are interpreted to reflect episodic organic carbon burial events [*Woodruff and Savin*, 1991]. Mi events represent inferred glacial maximums [*Miller et al.*, 1987; *Wright et al.*, 1992]. Changes in the oxygen isotope composition of seawater (δw) were identified by *Flower and Kennett* [1993]. Cli. optimum is climatic optimum.

1985] and strontium isotopic records [*Raymo*, 1994]. These arguments largely ignore changes in ocean circulation as a mechanism for climate change and assume that significant carbon removal from the atmosphere-ocean system led to global cooling during the middle Miocene and that elevated pCO_2 was responsible for the global warmth of the late early Miocene climatic optimum.

Evidence regarding a possible organic carbon burial control on pCO_2 can be found in carbonate $\delta^{13}C$ trends during the middle Miocene. Associated with a +1‰ shift recorded in the $\delta^{13}C$ of marine carbonates in the middle Miocene (Figure 1) is the occurrence of organic carbon-rich, circum-Pacific deposits such as the Monterey Formation of California [*Vincent and Berger*, 1985] and the marine phosphorite deposits of the southeastern United States coastal plain and shelf [*Compton et al.*, 1990]. The occurrence of a positive shift in carbonate $\delta^{13}C$ values coeval with the deposition of the Monterey Formation, followed by a positive shift in foraminiferal $\delta^{18}O$, suggests a possible sequence of increased rates of organic carbon burial, CO_2 removal, and consequent global cooling [*Vincent and Berger*, 1985]. Closer inspection of carbon isotope trends reveals shorter-term (~400 kyr) $\delta^{13}C$ excursions during the middle and late Miocene. The concentration of these events in the middle Miocene composes the fabric and overall character of the "Monterey excursion." These excursions, termed "carbon maxima" (CM) (Figure 1), are correlated with increased benthic foraminiferal $\delta^{18}O$ values and increased carbonate preservation, supporting a relationship between organic carbon burial, lower pCO_2, and bottom water cooling during this time [*Woodruff and Savin*, 1991].

Raymo [1994] challenged the claim that organic carbon burial was the primary agent of decreasing pCO_2 during the Miocene. On the basis of trends toward increasing $^{87}Sr/^{86}Sr$ (Figure 1) as a proxy for relative changes in rates of continental chemical weathering she argued for increasing silicate chemical weathering rates as the mechanism of CO_2 removal [*Raymo*, 1994]. The greatest rate of change in $^{87}Sr/^{86}Sr$, thus the greatest rate of proposed pCO_2 decrease, occurs during the early Miocene (~20-16 Ma) and is interpreted as reflecting rapid erosion of the Himalayan-Tibetan Plateau [*Hodell and Woodruff*, 1994; *Raymo*, 1994]. Furthermore, increased rates of chemical weathering would have resulted in increased nutrient influx, marine productivity, and organic carbon burial [*Raymo*, 1994]. However, in Raymo's model, decreasing pCO_2 during the Miocene is primarily driven by silicate weathering and not by organic carbon burial.

2. Site Descriptions, Sampling, and Stratigraphy

Samples from Deep Sea Drilling Project (DSDP) sites 588 (26°06.7'S, 161°13.6'E; southwest Pacific) and 608 (42°50.205'N, 23°05.252'W; North Atlantic) and Ocean Drilling Program (ODP) site 730 (17°43.885'N,

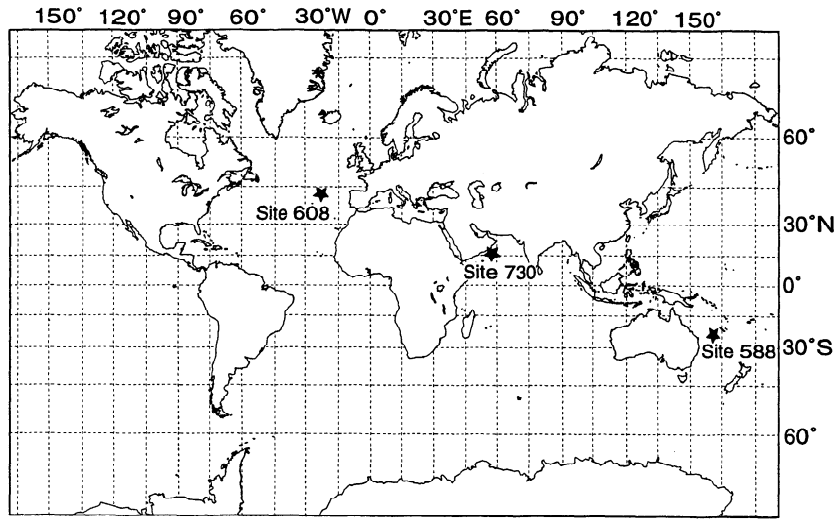

57°41.519'E; Oman margin, northwest Arabian Sea) were used to reconstruct pCO_2 for the late Oligocene to early late Miocene (~25-9 Ma) (Figure 2).

Initial sampling was designed to produce a temporal resolution of one sample per 100 kyr or less. However, recovery of alkenones varied stratigraphically, producing a variable temporal resolution at sites 588 and 608 and resulting in a highly aliased record in portions of the early to middle Miocene.

Low sedimentation rates (~2 cm kyr^{-1}) (Figure 3), characteristic low organic carbon (C_{org}) contents (0.1-0.01%) [*Pagani*, 1998], and predominance of nannofossil-foraminiferal oozes indicate that oligotrophic-type environments prevailed at sites 588 and 608 throughout the Miocene, whereas site 730, located on the Oman continental margin maintained comparatively higher rates of productivity. For example, middle Miocene sediments at site 730 are primarily foraminifer-bearing nannofossil chalk containing low C_{org} (0.6-0.1%) [*Pagani*,

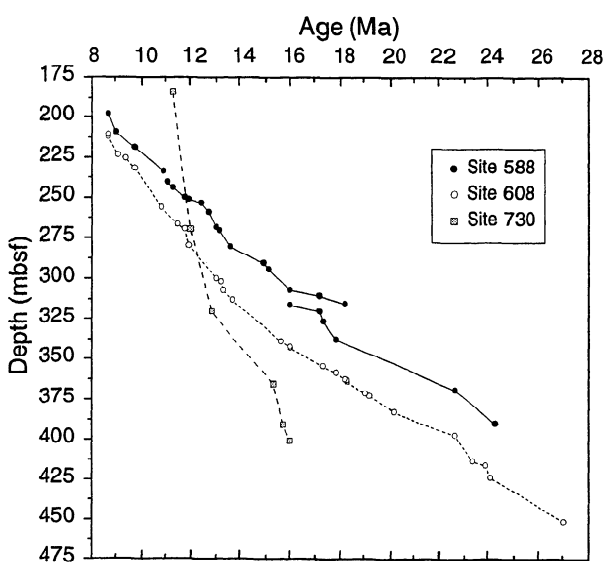

1998] and low to no siliceous microfossil content [*Shipboard Scientific Party*, 1989]. Age-depth plots indicate sedimentation rates ranged between 2.5 to 8.5 cm kyr^{-1} (Figure 3). These rates are 2-4 times higher than those found at sites 588 and 608. Although overall productivity was certainly higher on the Oman margin relative to sites 588 and 608, higher sedimentation rates are due, in part, to periodic emplacement of foraminifer-bearing turbidites and higher siliciclastic input [*Shipboard Scientific Party*, 1989]. The turbidites were avoided during sampling on the basis of visual examination.

Age models used for comparisons were developed by linearly interpolating between magnetostratigraphic, stable isotopic, biostratigraphic datums and by fitting linear segments to trends in Sr isotope analyses (Table 1). For this study, age datums are calibrated to the most recent geomagnetic polarity timescale (GPTS) [*Cande and Kent*, 1992; *Berggren et al.*, 1995]. Sites 588 and 608 have been extensively examined by other workers, allowing for rather precise correlations [*Clement and Robinson*, 1986; *Barton and Bloemendal*, 1986, *Wright et al.*, 1992; *Gartner*, 1992; *Hodell et al.*, 1991; *Hodell and Woodruff*, 1994].

The age model for site 730 is less constrained because of a lack of magnetostratigraphic data and few middle Miocene biostratigraphic datums. In an effort to improve age assignments, $^{87}Sr/^{86}Sr$ compositions of well-preserved planktonic foraminifera were measured, and age estimates (Table 1) were derived through comparison with strontium isotope-age curves constructed from sites 289 and 588 [*Hodell and Woodruff*, 1994].

3. Analytical Methods

Samples from DSDP/ODP were dried and weighed. Sediments were hydrated with distilled, deionized, and dichloromethane/hexane-extracted H_2O (5-10 mL), soaked in excess methanol for 10 min, and then subjected to Soxhlet extraction in a 2:1 azeotrope of dichloromethane and distilled methanol for 24 hours. A 5% NaCl solution was added to the total solvent extract to form two phases, and the neutral lipid

Table 1. Age Model Parameters

Site/Hole	Datum	Depth, m	Age, Ma	Reference [a]
588	Chron C4r.2r/C4An	198.3	8.70	1
588	Chron C4An/C4Ar.1r	205.1	9.03	1
588	Chron C4Ar.1r/C4Ar.1n	207.15	9.23	1
588	Chron C4Ar.1n/C4Ar.2r	209.45	9.31	1
588	Chron C4Ar.2r/C4Ar.2n	215.45	9.58	1
588	Chron C4Ar.2n/C4Ar.3r	217.55	9.64	1
588	Chron C4Ar.3r/C5n.1n	219.05	9.74	1
588	FAD *Coccolithus coalitus*	233.91	10.90	2,3
588A	Chron C5n.2n/C5r.1r	240.5	10.95	1
588A	CM7	244	11.30	4,4
588A	FAD *Discoaster kugleri*	250.1	11.80	2,3
588A	Chron C5r.3r/C5An.1n	251.35	11.94	1
588A	Chron C5An.1n/C5An.1r	253.6	12.08	1
588A	Chron C5An.2n/C5Ar.1r	259.35	12.40	1
588A	Chron C5Ar.3r/C5AAn	268.6	12.99	1
588A	Chron C5AAn/C5AAr	270.6	13.14	1
588A	LAD *Sphenolithus heteromorphous*	280.6	13.60	2,3
588A	FAD *Globorotalia peripheroacuta*	290.5	14.90	2,3
588A	FAD *Orbulina suturalis*	294.5	15.10	2,3
588A	CM3	307.25	16.00	5,6
588A	FAD *Globigerinoides bisphaericus*	310.6	17.15	2,3
588A	FAD *S. heteromorphous*	315.6	18.20	2,3
588C	CM3	316.1	16.00	4,6
588C	Mi-1b	337.8	17.80	7,6
588C	CM-O/M (end)	368.9	22.60	4,4
588C	Mi-1	388.8	23.90	7,6
588C	CM-O/M (beginning)	390	24.30	4,4
608	top Chron C4A	188.87	8.70	8
608	FAD *Discoaster loeblichii*	190.26	8.70	9,3
608	LAD *Discoaster bolli*	202.77	9.10	9,3
608	LAD *Discoaster hamatus*	204.98	9.40	9,3
608	top Chron C5	211.87	9.74	8
608	LAD *Coccolithus miopelagicus*	238.26	10.80	9,3
608	LAD *D. kugleri*	249.36	11.50	9,3
608	FAD *D. kugleri*	252.52	11.80	9,3
608	Chron C5/C5A	263.70	11.94	8
608	Chron C5A/C5AA	285.63	12.99	8
608	FAD *T. rugosus*	287.76	13.20	9,3
608	LAD *S. heteromorphous*	299.12	13.60	9,3
608	Chron C5AD/C5B	317.78	14.80	8
608	LAD *Helicosphaera ampliaperta*	327.66	15.60	9,3
608	Mi-2	331.40	16.00	7,6
608	Chron C5B/C5C	332.23	16.01	8
608	Chron C5C/C5D	344.69	17.28	8
608	Mi-1b	349.16	17.80	7,6
608	FAD *S. heteromorphous*	353.46	18.20	9,3
608	Chron C5D/C5E	353.94	18.28	8
608	LAD *Sphenolithus belemnos*	354.96	18.30	9,3
608	Chron C5E/C6	362.74	19.05	8
608	FAD *S. belemnos*	364.44	19.20	9,3
608	base Chron C6n	375.39	20.13	8
608	Chron C6/C6A	389.49	20.52	8
608	Chron C6A/C6AA	394.21	21.77	8
608	Chron C6AA/C6B	408.23	22.59	8
608	Mi-1	411.36	23.90	7,6
608	Chron C8/C9	449.64	27.03	8
608	LAD *Sphenolithus distentus*	455.08	27.50	9,3
730A	FAD *D. kugleri*	222.75	11.80	10,3
730A	87Sr/86Sr: 0.7088044	252.88	12.00	11
730A	87Sr/86Sr: 0.708793	307.55	12.80	11
730A	87Sr/86Sr: 0.7087567	356.56	15.30	11
730A	87Sr/86Sr: 0.7087182	383.96	15.70	11
730A	87Sr/86Sr: 0.7087133	394.86	16.00	11

FAD = first appearance datum; LAD = last appearance datum.

[a] The first number of the reference column refers to the identification of the datum level, the second number refers to the age assignment: (1) *Barton and Bloemendal* [1986], (2) *Jenkins and Srinivasan* [1986], (3) *Berggren et al.* [1985], (4) *Hodell and Woodruff* [1994], (5) *Flower and Kennett* [1993], (6) *Oslick et al.* [1994], (7) *Wright et al.* [1992], (8) *Clement and Robinson* [1987], (9) *Gartner* [1992], (10) *Spaulding* [1991], and (11) This study.

fraction in the dichloromethane phase was isolated by separatory funnel. The remaining aqueous and methanol phase was washed three more times with dichloromethane, and the resulting neutral lipid fractions were collected and combined. The resulting total lipid extract was separated into compound classes by silica gel column chromatography. Compound abundances were determined using a Hewlett Packard 5890 Series II gas chromatograph fitted with an on-column injector to a fused silica, DB-1 phase column (60 m x 0.32 mm ID, 0.25 μm film thickness). The temperature program was 60°-200°C at 20°C min^{-1}, then 200°-320°C at 5°C min^{-1} (isothermal for 35 min). Heptatriaconta-15E, 22E-dien-2-one (diunsaturated alkenone) was identified by gas chromatography/mass spectrometry (GC/MS) and subsequently identified by comparison of elution times.

In this study, most triunsaturated alkenones ($C_{37:3}$) are below limits of instrument detection. If unaltered, $U^{K'}_{37}$ temperature estimates (using the calibration of *Prahl and Wakeham* [1987]) are relatively invariant and significantly high (~30°C) at all sites compared to those derived from $\delta^{18}O$ of planktonic foraminifera. This implies either (1) the modern $U^{K'}_{37}$ calibration is not applicable to the Miocene or (2) the triunsaturated form has been preferentially degraded, which is consistent with studies of alkenone diagenesis in Miocene and Pliocene sediments [*Hoefs et al.*, 1998].

The extracted sediment was washed under distilled and deionized H_2O, sonicated, and sieved into <60, 150-250, 250-354, and 354-420 μm size fractions. Single species and/or genera of planktonic foraminifera were picked from the 250-354 and 354-420 μm size fractions. Some samples contained fine-fraction carbonate contaminants and required additional treatment. These samples were treated with hot H_2O_2 (30-20%), washed, and repeatedly sonicated in deionized H_2O.

Compound-specific isotope analyses were performed using a GC combustion system connected to a Finnigan modern analog technique (MAT) 252 mass spectrometer [*Merritt et al.*, 1995]. Compounds eluting from a gas chromatograph are combusted over nickel and platinum at 1000°C. Water is removed through a refrigerated Nafion permeable membrane [*Leckrone and Hayes*, 1997] and is externally flushed with helium; the resulting purified CO_2 is introduced into the mass spectrometer. Isotopic compositions are calculated relative to Peedee belemnite (PDB) by comparison with a gas standard calibrated to National Bureau of Standards (NBS) -19 and by assigning a value of 1.95‰ for $\delta^{13}C$ [*Ricci et al.*, 1994]. Analytical uncertainty determined by multiple measurements of coinjected standards is ±0.67‰.

Stable isotope compositions of planktonic foraminifera were analyzed on a Finnigan MAT 252 mass spectrometer with an automated common acid bath system. Each sample was reacted with 100% phosphoric acid at 90°C. Carbon and oxygen isotopic values are reported in δ notation as per mill (‰) deviation from the Vienna Peedee belemnite (VPDB) standard. NBS-19 was used as the calibration standard assigning a value of 1.95 and -2.2‰ for $\delta^{13}C$ and $\delta^{18}O$, respectively. Analytical uncertainty for $\delta^{13}C$ and $\delta^{18}O$ values, determined by analysis of carbonate standards, is 0.05‰ and 0.13‰, respectively.

Strontium isotope compositions were measured on a Finnigan MAT 262 mass spectrometer equipped with a scanning electron microscope and six faraday detectors by L. Derry at Cornell University. All data were normalized to a constant National Institute of Standards and Technology (NIST) standard NIST-987 = 0.710235 on the basis of the measured value of NIST-987 determined for each series of analyses. Analytical error determined by repeated analyses of NIST-987 is $\pm 4 \times 10^{-5}$ (2σ).

4. Approach to Paleo-pCO_2 Reconstruction

Published attempts to quantify the relationship between $CO_{2(aq)}$ and $\delta^{13}C_{org}$ have resulted in an array of empirically derived calibrations [*McCabe*, 1985; *Rau et al.*, 1989, 1991; *Hollander and McKenzie*, 1991; *Jasper and Hayes*, 1990; *Jasper et al.*, 1994; *Freeman and Hayes*, 1992; *Hinga et al.*, 1994]. Recent theoretical consideration [*Rau et al.*, 1992, 1996; *Francois et al.*, 1993; *Goericke et al.*, 1994] and experimental work demonstrated that cellular growth rate [*Laws et al.*, 1995; *Bidigare et al.*, 1997] and cell geometry [*Popp et al.*, 1998a] also exert considerable control on $\delta^{13}C_{org}$ insofar as they influence the intracellular CO_2 concentration available for carbon fixation. If one assumes that intracellular $CO_{2(aq)}$ is supplied by diffusion, then the magnitude of carbon isotope discrimination that occurs during photosynthesis (ε_p) can be expressed as a function of the isotope fractionations associated with carbon transport and fixation as well as the concentrations of $CO_{2(aq)}$ external and internal to the cell [*Farquhar et al.*, 1982]. The slope of a line, generated by plotting ε_p versus $1/CO_{2(aq)}$ can be empirically derived for specific organisms [*Laws et al.*, 1995; *Bidigare et al.*, 1997]. Thus the expression for ε_p can be simplified as

$$\varepsilon p = \varepsilon f - \frac{b}{Ce} \quad (1)$$

where ε_f is the carbon isotope fractionation associated with carbon fixation, C_e is the concentration of $CO_{2(aq)}$ external to the cell, and b is the sum of physiological factors affecting the total carbon discrimination such as growth rate [*Rau et al.*, 1989; *Francois et al.*, 1993; *Laws et al.*, 1995; *Bidigare et al.*, 1997] and cell geometry [*Rau et al.*, 1996; *Popp et al.*, 1998a]. There are additional physiological controls on carbon uptake and carbon isotope discrimination during algal photosynthesis. These include differences in carbon substrate and enzymes used during carbon fixation [see *Goericke et al.*, 1994] and CO_2 concentrating mechanisms [*Sharkey and Berry*, 1985; *Falkowski*, 1991; e.g., *Raven and Johnston*, 1991].

In summary, there is a potential to extract a history of surface water [$CO_{2(aq)}$] from marine organic matter because the isotopic fractionation that occurs during photosynthesis is primarily a function of [$CO_{2(aq)}$] and growth rate. However, complicating this approach are an array of isotopic signals from terrestrial organic matter contamination and marine photosynthesizers with varying carbon fixation pathways and cell geometries that are integrated in bulk sedimentary organic matter. One can be confident of analyzing carbon derived exclusively from marine organic sources by utilizing certain organic molecules derived from known marine sources. When these molecules or their derivatives (biomarkers) are unique to a particular class of organisms, the range of metabolic pathways and cell geometries affecting the carbon isotopic charac-

ter is narrowed. In this context, C_{37} alkenones are excellent biomarkers. Exclusive to some haptophyte algae [*Volkman et al.*, 1980; *Marlowe et al.*, 1984; *Conte et al.*, 1994], alkenones are well known for their utility in the $U^{K'}_{37}$ temperature proxy [e.g., *Brassell et al.*, 1986] and can act as isotopic recorders of surface water conditions. Furthermore, haptophytes have a narrow range of cell geometries and diameters [see *Bidigare et al.*, 1997; *Popp et al.*, 1998a], thereby minimizing this variable as a significant control on isotopic compositions.

In accordance with the above discussion this study utilizes the $\delta^{13}C$ compositions of diunsaturated alkenones ($\delta^{13}C_{37:2}$) and carbonate from near-surface-dwelling foraminifera to calculate ε_p and reconstruct paleo-pCO_2 during the Miocene. This methodology has been used effectively to evaluate paleoceanographic dynamics and surface water [$CO_{2(aq)}$] during the Pleistocene [*Jasper and Hayes*, 1990; *Jasper et al.*, 1994]. Recent experimental results for *Emiliania huxleyi* also have shown ε_p, determined from diunsaturated alkenones ($\varepsilon_{p37:2}$), to be correlated to growth rate and [$CO_{2(aq)}$] [*Bidigare et al.*, 1997]. The same study, using empirical observations from five environmentally diverse, low-latitude Pacific sites, calibrated $\varepsilon_{p37:2}$ as a function of surface water [PO_4^{3-}] and [$CO_{2(aq)}$]. In these open ocean settings, haptophyte growth rates are most likely responding to changes in the availability of trace metal micronutrients, which covary with [PO_4^{3-}] [*Bidigare et al.*, 1997]. Accordingly, reconstruction of paleo-$CO_{2(aq)}$, requires knowledge of ancient growth rates, for which there is no proxy, or estimation of surface water [PO_4^{3-}] from which growth rates may be inferred. Our approach is to develop $\varepsilon_{p37:2}$ records from ostensibly low-productivity, stable oceanographic settings. In this way, large-scale variations in growth rates and surface-water [PO_4^{3-}] are minimized, allowing [$CO_{2(aq)}$] to dominate records of ε_p. In addition, these oceanographic settings have low air-to-sea disequilibrium in respect to CO_2, allowing a more accurate estimation of Miocene pCO_2.

4.1. Calculation of ε_p

Calculation of ε_p requires knowledge of the carbon isotopic composition of haptophyte biomass ($\delta^{13}C_{org}$) and $CO_{2(aq)}$ ($\delta^{13}C_{CO2(aq)}$). Culture experiments have determined the isotopic difference between haptophyte biomass and $C_{37:2}$ alkenones ($\varepsilon_{alkenone}$) to be ~4‰, with alkenones depleted relative to total organic biomass [e.g., *Bidigare et al.*, 1997; *Popp et al.*, 1998b]. The $\delta^{13}C_{CO2(aq)}$ value is reconstructed from the carbon isotope composition of shallow-dwelling foraminifera. This approach assumes isotopic and chemical equilibria prevailed among all the carbon aqueous species and atmospheric CO_2 as well as foraminiferal calcite. However, additional metabolically related fractionations are known to occur in planktonic foraminifera [*Spero and DeNiro*, 1987; *Spero and Lea*, 1993]. These effects, commonly ascribed to species hosting algal symbionts, can cause foraminiferal $\delta^{13}C$ values to be ~0.5-1.5‰ enriched in ^{13}C relative to species unaffected by algal symbiont photosynthesis [*Spero and DeNiro*, 1987; *Bijima*, 1990; *Spero and Lea*, 1993]. For this study, disequilibrium carbon isotopic enrichments of 0.5-1.0‰ would similarly increase values of ε_p and increase estimated pCO_2. However, variations of this magnitude would have a minimal impact on estimated pCO_2 and would not alter our interpretations.

From the above discussion all necessary terms including δ_{org}, $\delta^{13}C_{CO2(g)}$, $\delta^{13}C_{CO2(aq)}$, and $\varepsilon_{p37:2}$ can be determined from the following relationships:

$$\varepsilon_{alkenone} \approx -4.2 = [(\delta_{37:2} + 1000)/(\delta_{org} + 1000)-1]10^3 \quad (2)$$

$$\varepsilon_{calcite\text{-}CO2(g)} = [(\delta_{calcite} + 1000)/(\delta_{CO_2(g)} + 1000)-1]10^3 \quad (3)$$

$$\varepsilon_{CO_2(aq)\text{-}CO2(g)} = [(\delta_{CO_2(aq)} + 1000)/(\delta_{CO_2(g)} + 1000)-1]10^3 \quad (4)$$

$$\varepsilon_{p37:2} = [(\delta_{CO_2(aq)} + 1000)/(\delta_{org} + 1000)-1]10^3 \quad (5)$$

where the temperature-dependent fractionation factors relating foraminifera calcite to $CO_{2(g)}$, and $CO_{2(aq)}$ to $CO_{2(g)}$ (determined by *Romanek et al.*, [1992] and *Mook et al.*, [1974], respectively) are

$$\varepsilon_{calcite\text{-}CO2(g)} = 11.98 - 0.12 \times T(°C) \quad (6)$$

$$\varepsilon_{CO_2(aq)\text{-}CO2(g)} = -373/T(°K) + 0.19 \quad (7)$$

Because the carbon isotopic range of alkenones is much greater than that measured from surface-dwelling planktonic foraminifera, the character of $\varepsilon_{p37:2}$ is largely determined by relative variation in $\delta^{13}C_{37:2}$ values. The traits of these $\varepsilon_{p37:2}$ trends are very similar to those previously described for the $\delta^{13}C_{37:2}$ records.

4.2. Calculation of pCO_2

Modern ocean $\varepsilon_{p37:2}$ values have been calibrated to surface water [$CO_{2(aq)}$], [PO_4^{3-}], and haptophyte growth rates [*Bidigare et al.*, 1997, 1999; *B. N. Popp*, unpublished data, 1999]. The results of measurements from locations in the Pacific, Atlantic, and Indian Oceans (n=80) provide the following relationship:

$$b_{(37:2)} = 116.96[PO_4^{3-}] + 81.42 \quad (8)$$

(Note: derivation assumes ε_f = 25‰; see below). Equation (8) in combination with (1) allows the calculation of [$CO_{2(aq)}$] if [PO_4^{3-}] is known or approximated. An additional consideration in the evaluation of ancient CO_2 concentrations is the value assigned to the maximum isotopic fractionation attributed to enzymatic fixation (ε_f). Maximum fractionation will be obtained at high ambient concentrations of [$CO_{2(aq)}$] and/or as growth rate approaches zero. A value of 29‰ for the in vitro fractionation factor associated with the enzyme Rubisco (ribulose-1,5-biphosphate carboxylase/oxygenase) with respect to aqueous CO_2 has broad agreement [*Roeske and O'Leary*, 1984; e.g., *Raven and Johnston*, 1991]. However, this value is rarely attained for marine phytoplankton. The relatively smaller in situ fractionation (~27‰ for haptophytes) [see *Wong and Sackett*, 1978; references therein] has been attributed to a contribution of β-carboxylase, phosphoenolpyruvate-carboxylase (PEPC), to the total carbon fixation [*Farquhar and Richards*, 1984], and/or active carbon transport to the site of fixation [*Sharkey and Berry*, 1985; *Falkowski*, 1991; *Raven and Johnston*, 1991]. *Goericke et al.* [1994] calculate a general range of 25.4-28.3‰ for ε_f in algae with C_3-type metabolisms, considering a 2-10% contribution of β-carboxylation to the total carboxylation.

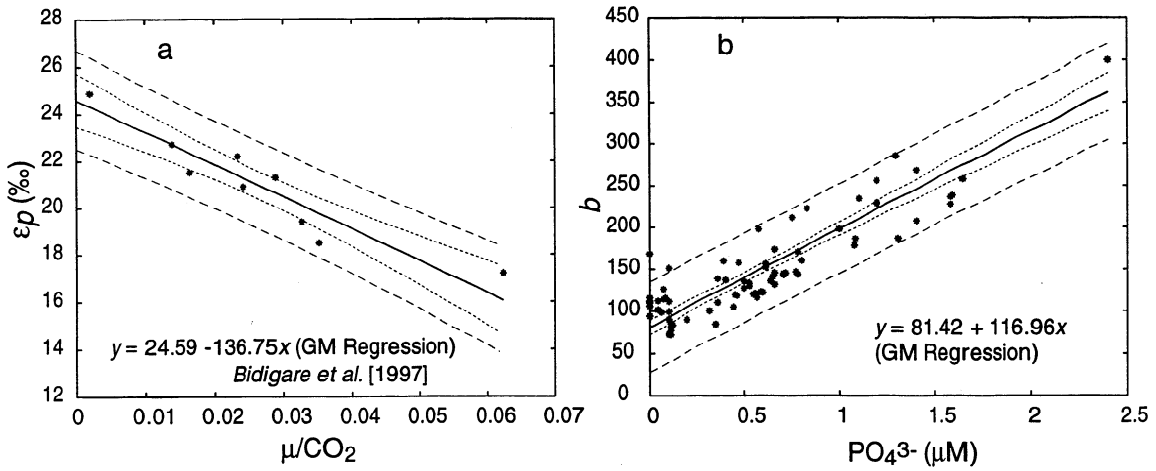

Figure 4. (a) ε_p versus μ/CO_2 for chemostat cultures of haptophyte algae. Data are from *Bidigare et al.* [1997]. The solid line represents geometric mean regression. The dotted lines reflect 95% confidence intervals. The dashed lines represent prediction bands that capture 95% of the entire data. The y intersections represent theoretical values of ε_f. (b) Compilation of b versus $[PO_4]$ using data of *Bidigare et al.* [1997, 1999] and *B.N. Popp*, (unpublished data, 1999). Values for b are calculated using a value of 25‰ for ε_f. The solid line represents the geometric mean regression. The dotted lines reflect 95% confidence intervals. The dashed lines represent prediction bands that capture 95% of entire data.

Recent chemostat experiments performed on *Phaeodactylum tricornutum* [*Laws et al.*, 1995], *Porosira glacialis* [*Popp et al.*, 1998a], and two strains of *E. huxleyi* [*Bidigare et al.*, 1997] conclude that the in situ fractionation due to the combined effects of Rubisco and β-carboxylase carboxylations is ~25‰ for these strains. The *Bidigare et al.* [1997] results are shown in Figure 4a, with ε_p plotted against the ratio of growth rate and $[CO_{2(aq)}]$. The geometric mean regression is bracketed by 95% confidence intervals, as well as more conservative prediction bands (which capture 95% of the entire data). This approach is admittedly conservative; however, it demonstrates that a wider range for ε_f (22.5-26.6‰) is statistically plausible. Therefore, because physiological characteristics of ancient organisms cannot be precisely known, consideration of available data suggests a range of 25-27‰ for ε_f is appropriate for the calculation of paleo-$[CO_{2(aq)}]$. This range does not greatly alter calculated pCO_2 since pCO_2 values are <15 ppmv higher if a value of 27, rather than 25, is used for ε_f.

A reevaluation of the term b is handled in a similar manner (Figure 4b). Table 2 lists the equations derived for the geometric mean regressions and the 95% confidence level curves calculated using 25 and 27‰ for ε_f.

We selected a range of phosphate concentrations in order to calculate Miocene $[CO_{2(aq)}]$. The majority of haptophyte productivity likely occurred in the upper 100 m of the photic zone at site 588, where today the $[PO_4^{3-}]$ ranges from 0.2 μM at 50 m to 0.3 μM at 100 m (http://ferret.wrc.noaa.gov/fbin/climate_server). Site 608 has slightly higher $[PO_4^{3-}]$ at 100 m (~0.35 μM). Phosphate concentrations during the Miocene could have diverged both globally and regionally from modern distributions [*Delaney*, 1990]. This is particularly true for site 730, which would have experienced dramatic alteration in the distribution of nutrients in the upper water column following the development of monsoonal upwelling. Conversely, the lithologic and sediment accumulation record at site 588 can be interpreted as reflecting oceanographic stability throughout the Miocene. Export production appears uniformly low during this time, supporting low nutrient availability. Consequently, for site 588 the modern range of 0.2-0.3 μM is considered applicable during the Miocene.

Paleo-$[PO_4^{3-}]$ at sites 608 and 730 are more difficult to evaluate. Site 608 likely experienced changes in water column stability throughout the early to middle Miocene (see below), and it is impossible to estimate how these changes affected the relative concentrations of nutrients through time. Because the overall sedimentological and oceanographic character of sites 588 and 608 are similar (i.e., sedimentation rates, C_{org}, and lithology), we assume that on average, $[PO_4^{3-}]$ was similar.

Table 2. Equations Used to Calculate $[CO_{2(aq)}]$

	GM Regression	95% Confidence Interval (upper)	95% Confidence Interval (lower)
$\varepsilon_f = 25$	$\frac{[(116.96[PO4]) + 81.42]}{(25 - \varepsilon_p)}$	$\frac{[(4.17[PO4]^2) + (113.79[PO4]) + 88.63]}{(25 - \varepsilon_p)}$	$\frac{[(-4.17[PO4]^2) + (120.14[PO4]) + 74.21]}{(25 - \varepsilon_p)}$
$\varepsilon_f = 27$	$\frac{[(128.96[PO4]) + 101.37]}{(27 - \varepsilon_p)}$	$\frac{[(4.35[PO4]^2) + (125.65[PO4]) + 108.89]}{(27 - \varepsilon_p)}$	$\frac{[(-4.35[PO4]^2) + (132.27[PO4]) + 93.85]}{(27 - \varepsilon_p)}$

GM regression refers to geometric mean regression. Equations for GM regressions and the upper/lower 95% confidence intervals for ε_f = 25 and 27‰ are calculated using all available data of b versus $[PO_4]$ for the modern ocean.

For site 730, we assume a premonsoon range of 0.3-0.4 μM because inferred productivity levels were higher in the northern Arabian Sea than in either the southwest Pacific Ocean or North Atlantic sites.

We calculated paleo-[$CO_{2(aq)}$] on the basis of the assumptions and estimates discussed above. These values were then converted to atmospheric CO_2 concentrations by assuming air-sea equilibrium and applying Henry's Law:

$$pCO_2 = [CO_{2(aq)}]/K_H \quad (9)$$

where K_H is the temperature- and salinity-dependent CO_2 solubility coefficient [*Weiss*, 1974]. K_H for each sample was calculated assuming a salinity of 35 and applying surface water temperatures derived from $\delta^{18}O$ of planktonic foraminifera.

4.3. Sources of Uncertainty in pCO_2 Calculations

4.3.1. Molecular diagenesis. Of significance to this study is whether isotopic alteration occurs within a suite of molecules such as $C_{37:2}$ alkenones. In general, the degree of unsaturation affects reactivity rates, with highly unsaturated compounds appearing more labile [*Cranwell et al.*, 1987]. However, this does not seem to apply to alkenone reactivity. The relatively refractory nature of unsaturated alkenones is demonstrated in its occurrence throughout sediments of Cenozoic age [e.g., *Brassell*, 1993] and is attributed to their unusual trans configuration, a molecular architecture that may inhibit bacterial biodegradation [*Rechka and Maxwell*, 1988].

Although few studies have addressed the effects of diagenesis on the carbon isotopic composition of specific molecules, it is generally assumed that alteration is negligible. *Hayes et al.* [1990] discussed theoretical considerations and argued that the similarity among isotope compositions of Cretaceous-aged porphyrins with varying carbon numbers was evidence for a lack of isotopic diagenesis. Further, a consistent isotopic offset (averaging ~4.5‰) between porphyrins and isoprenoids extracted from the Cretaceous Greenhorn Formation [*Hayes et al.*, 1990] is similar to the range observed in living organisms, thus supporting isotopic preservation of both sets of compounds. *Huang et al.* [1997] measured no change in the carbon isotope composition of individual *n*-alkanes from a 23 year decomposition experiment of *Calluna vulgaris*, although over 90% of the original compounds were degraded. *Freeman et al.* [1994] found no strong evidence for isotopic fractionation associated with diagenetic aromatization of polycyclic aromatic hydrocarbons from the Eocene Messel Shale.

Given the available research, there is little reason to suspect diagenetic alteration. Therefore the trends and absolute $\delta^{13}C_{37:2}$ values in this study are taken to represent the carbon isotopic compositions of haptophyte lipids from which biomass $\delta^{13}C$ values can be estimated.

4.3.2. Active carbon transport. Calculations of [$CO_{2(aq)}$] and pCO_2 are predicated on the assumption of the diffusive transport of inorganic carbon to the site of fixation. If the dominant haptophyte population during the Miocene had the ability to concentrate inorganic carbon, isotopic compositions and the expression of ε_p would be affected. Some extant haptophytes, such as *Isochrysis galbana*, appear to have the ability to actively transport inorganic carbon [*Burns and Beardall*, 1988; see *Raven and Johnston*, 1991]. Furthermore, physiological differences have been detected between low- and high-calcifying strains of *E. huxleyi* [*Nimer and Merrett*, 1992; *Nimer et al.*, 1992]. High-calcifying strains of *E. huxleyi* contain carbonic anhydrase [*Quiroga and Gonzalez*, 1993; *Nimer et al.*, 1994], an enzyme that catalyzes the reversible hydration of carbon dioxide [*Tsuzuki and Miyachu*, 1989]. However, there is no evidence for a CO_2 concentrating mechanism in either strain [*Nimer and Merrett*, 1992; *Bidigare et al.*, 1997]. For *E. huxleyi* the $K_{0.5[CO2]}$ (i.e., the concentration of ambient CO_2 required to achieve 50% of the maximum photosynthetic growth rate) is 15-20 μM at a *p*H of 8.0-8.3 [*Nimer and Merrett*, 1992; *Nimer et al.*, 1992]. Though this implies that ambient carbon concentrations in natural settings may limit growth, it does not preclude low, sustained growth at lower [$CO_{2(aq)}$]. The results of other chemostat growth experiments [*Bidigare et al.*, 1997] are consistent with a model of diffusive transport of inorganic carbon under low [$CO_{2(aq)}$] (<10 μM) for both high- and low-calcifying strains of *E. huxleyi*. Significantly, ε_p values in these experiments were indistinguishable between strains for a variety of growth rates and [$CO_{2(aq)}$].

4.3.3. Carbonate diagenesis, temperature considerations, and δw. Calculations of both $\delta^{13}C_{CO2(aq)}$ and pCO_2 require an assumption of chemical and isotopic equilibrium and accurate records of environmental temperatures. For this study, surface water temperatures were calculated from the $\delta^{18}O$ compositions of shallow-dwelling planktonic foraminifera in combination with a changing seawater $\delta^{18}O$ composition (δw). This approach requires the assumption that foraminiferal growth and calcification occurred at the same water depth as haptophyte production. Because CO_2 solubility increases with decreasing temperatures, estimates of pCO_2 would be in error on the high side if alkenone production occurred deeper relative to foraminifera growth. Although only well-preserved foraminifera tests were measured, the possibility exists that diagenetic processes caused relatively minor alteration of primary isotopic compositions. These processes, including differential dissolution, reprecipitation, and carbonate infilling, would actually tend to enrich foraminiferal $\delta^{18}O$ compositions [*Schrag et al.*, 1992], thus registering lower $\delta^{18}O$-based temperature estimates and leading us to underestimate pCO_2. The potential effect of carbonate diagenesis on our final pCO_2 record is discussed in section 6.1 but is considered minimal.

Accurate calculation of ancient surface water temperatures requires an estimation of temporal changes in δw. *Shackleton and Kennett* [1975] calculated a value of -1‰ (SMOW) for δw assuming little to no glacial ice. Although a large Antarctic ice sheet has not been demonstrated for the pre-middle Miocene, significant expansion and contraction of ice volumes has been documented for the early Miocene [*Miller et al.*, 1987; *Miller and Sugarman*, 1995; *Zachos et al.*, 1997]. Proposed changes in δw during these glacial episodes are estimated to range between 0.5 and 1.0‰ (SMOW) [*Miller et al.*, 1987, *Zachos et al.*, 1997] and are considered in our final calculations of pCO_2.

The character of the middle Miocene $\delta^{18}O$ shift has been analyzed in detail from high-resolution, stable isotope records at site 588 [*Flower and Kennett*, 1993]. Interpreting the covariance between benthic (*Cibicidoides* spp.), surface-dwelling (*Globigerinoides quadrilobatus*), and deep-dwelling planktonic (*Globoquadratus dehiscens*) foraminiferal $\delta^{18}O$, *Flower and Kennett* [1993] conclude that the mid-

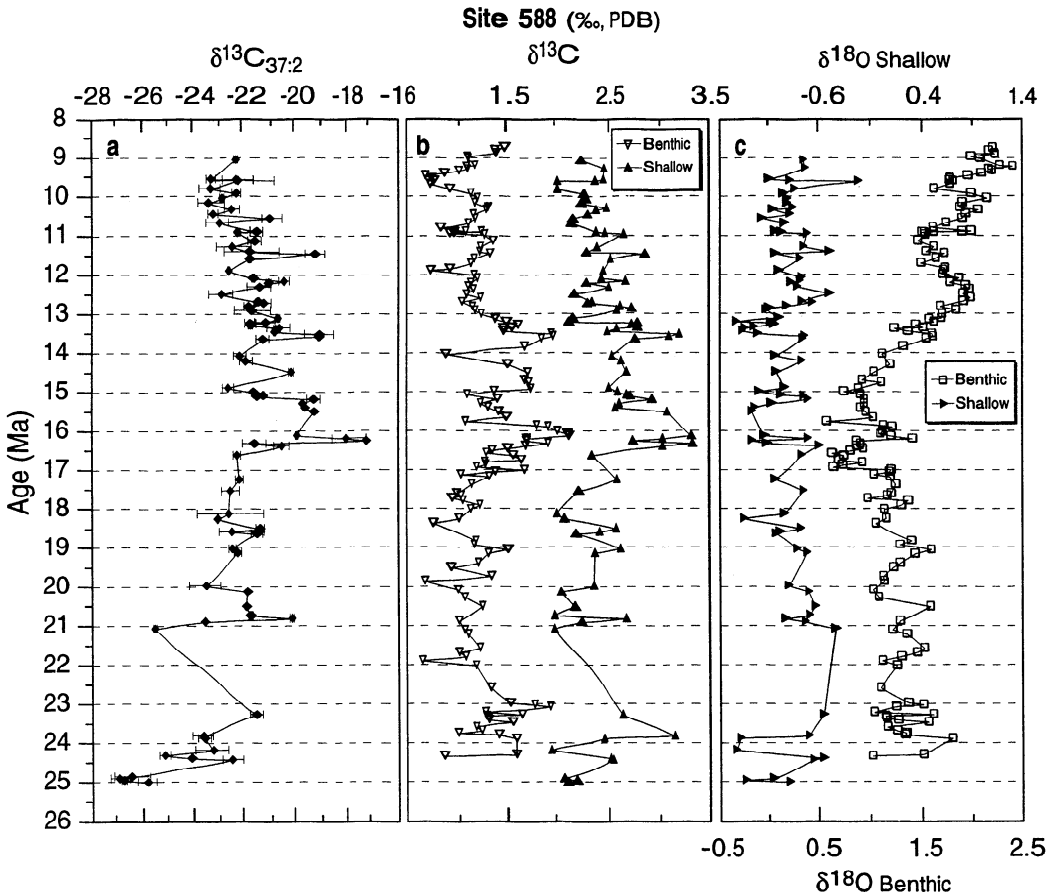

Figure 5. Total isotope data from site 588. Diunsaturated alkenones (solid diamonds), surface-dwelling planktonic foraminifera ($\delta^{13}C$; vertical solid triangles; $\delta^{18}O$; horizontal solid triangles), and benthic foraminifera ($\delta^{13}C$; inverted open triangles; and $\delta^{18}O$; open squares). Data for benthic foraminifera are from *Kennett* [1985].

dle Miocene +$\delta^{18}O$ shift occurred in several steps: a +0.2‰ shift between ~14.6 and 14.0 Ma, a +0.5‰ shift from ~13.6 to 13.55 Ma, and a +0.3‰ shift from 12.5 to 12.1 Ma (Figure 1). Applying their conclusions and assuming an invariant seawater relative salinity of 35, and a value of -1‰ (SMOW) for the δw prior to EAIS growth [*Shackleton and Kennett*, 1975], we calculate records of mixed layer temperatures at all three sites. These temperature estimates are then applied in the calculation of pCO_2 (discussed below). It is important to note that the application of a +1‰ shift in seawater +$\delta^{18}O$ causes calculated surface water temperatures to rapidly increase, which subsequently drives an increase in calculated pCO_2 across these intervals.

4.3.4. Miocene ε_p versus $CO_{2(aq)}$ calibration. It is possible, though difficult to prove or quantify, that the relationship between $\varepsilon_{p37:2}$ and surface water $CO_{2(aq)}$ during the Miocene was different than the modern calibration discussed above. Differences can be potentially attributed to factors such as a decoupling between growth rate-limiting micronutrients and [PO_4^{3-}] and differences in the average cell volume to surface area ratio in alkenone-producing haptophytes during the Miocene. The potential errors attributable to these effects are evaluated in the final discussion.

5. Results

Isotopic trends for diunsaturated alkenones, shallow-dwelling planktonic foraminifera, and benthic foraminifera are shown in Figures 5-7. Using $\delta^{18}O$ values of shallow-dwelling planktonic foraminifera, mixed layer temperatures are calculated (Figure 8) and records of $\varepsilon_{p37:2}$ are reconstructed (Figure 9). Importantly, the range of $\delta_{37:2}$ variation is far greater than that recorded in foraminiferal $\delta^{13}C$. Thus the overall trends of $\varepsilon_{p37:2}$ at these sites are predominantly controlled by $\delta_{37:2}$.

In general, the long-term trends and average values of $\varepsilon_{p37:2}$ between sites 588, 608, and 730 are similar (Figure 9), although distinctive differences exist. At site 588, low $\varepsilon_{p37:2}$ values and CM events are closely associated. The lowest $\varepsilon_{p37:2}$ values occur across the Monterey excursion corresponding to events CM3, CM4, and CM6. At site 608, $\varepsilon_{p37:2}$ values do not appear to track CM events except for CM1 and CM5, which correlate with negative $\varepsilon_{p37:2}$ excursions of ~5 and 4.6‰, respectively (Figure 9a).

Clearly, the timing and magnitude of $\varepsilon_{p37:2}$ excursions between 18 and 15 Ma recorded in the North Atlantic deviate from those recorded in the southwest Pacific. Site 608 con-

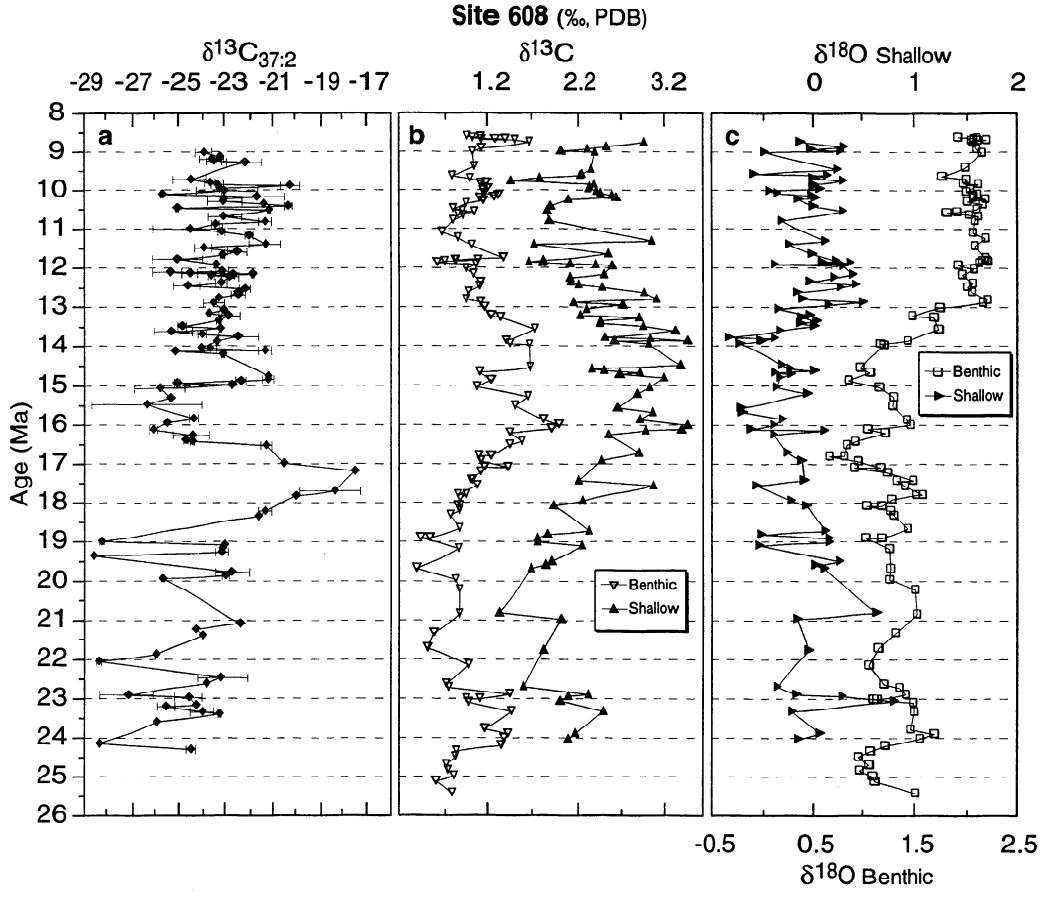

Figure 6. Total isotope data from site 608. See Figure 5 caption for details. Data for benthic foraminifera are from *Wright et al.* [1991, 1992].

tains a -3.8‰ shift from 18.1 to 16.9 Ma, resulting in the lowest $\varepsilon_{p37:2}$ values occurring within the measured interval. A similar excursion is recorded from site 588 but occurs ~700 kyr later. At site 608 the negative $\varepsilon_{p37:2}$ shift is rapidly reversed with a 9.4‰ increase occurring between 16.9 and 15.8 Ma.

Average $\varepsilon_{p37:2}$ values from site 730 in the Arabian Sea are very similar to site 588 (Figure 9b). Weaker stratigraphic control at site 730 prevents detailed comparisons. However, longer-term trends between sites 730 and 588 show a close correspondence. In general, lower ε_p values occur from ~16.2 to 15.1 Ma at both sites, with the lowest values roughly coinciding with carbon maxima events CM4-CM6.

Estimates for pCO_2 (Figure 10) are calculated using the equations derived from the data of *Bidigare et al.* [1997, 1999] (Table 2). Maximum (ε_f = 27‰; $[PO_4^{3-}]$ = 0.3 μM) and minimum (ε_f = 25‰; $[PO_4^{3-}]$ = 0.2 μM) values are bracketed for Figures 10a-10c. Results from all three sites evaluated in this study suggest atmospheric carbon dioxide concentrations were at or below pre-industrial values (290 ppmv), with most of the early and middle Miocene maintaining pCO_2 values between Pleistocene glacial/interglacial intervals (~290-190 ppmv). Details and implications of the pCO_2 trends are discussed below.

6. Discussion

6.1. Consideration of Error

Alkenone isotope compositions from sites 588, 608, and 730 are not remarkably different from those measured in other studies (Figure 11). In comparison with Pleistocene samples, Miocene ε_p values are lower by 2-3‰. Under low pCO_2 conditions, relatively large site to site differences in $\varepsilon_{p37:2}$ (i.e., 5‰) can be driven by minor differences in $[CO_{2(aq)}]$ and haptophyte growth rates. If, as we suggest, similar atmospheric CO_2 concentrations prevailed for these time periods, these small isotopic differences are readily attributable to physical oceanographic properties and/or nutrient concentrations between sites. In addition, there is relative consistency among the range and trends of $\delta^{13}C_{37:2}$ and $\varepsilon_{p37:2}$ values from the three sites measured in this study. It would be fortuitous if this agreement were driven by diagenetic processes, and as discussed previously, there is little reason to suspect alkenone carbon isotopic compositions have been greatly altered.

Legitimate estimates of paleo-pCO_2 are predicated on the assumption of diffusive carbon flux to the site of carbon fixation within algal cells. However, the physiology of Miocene haptophytes is unknown. One could speculate that if modern

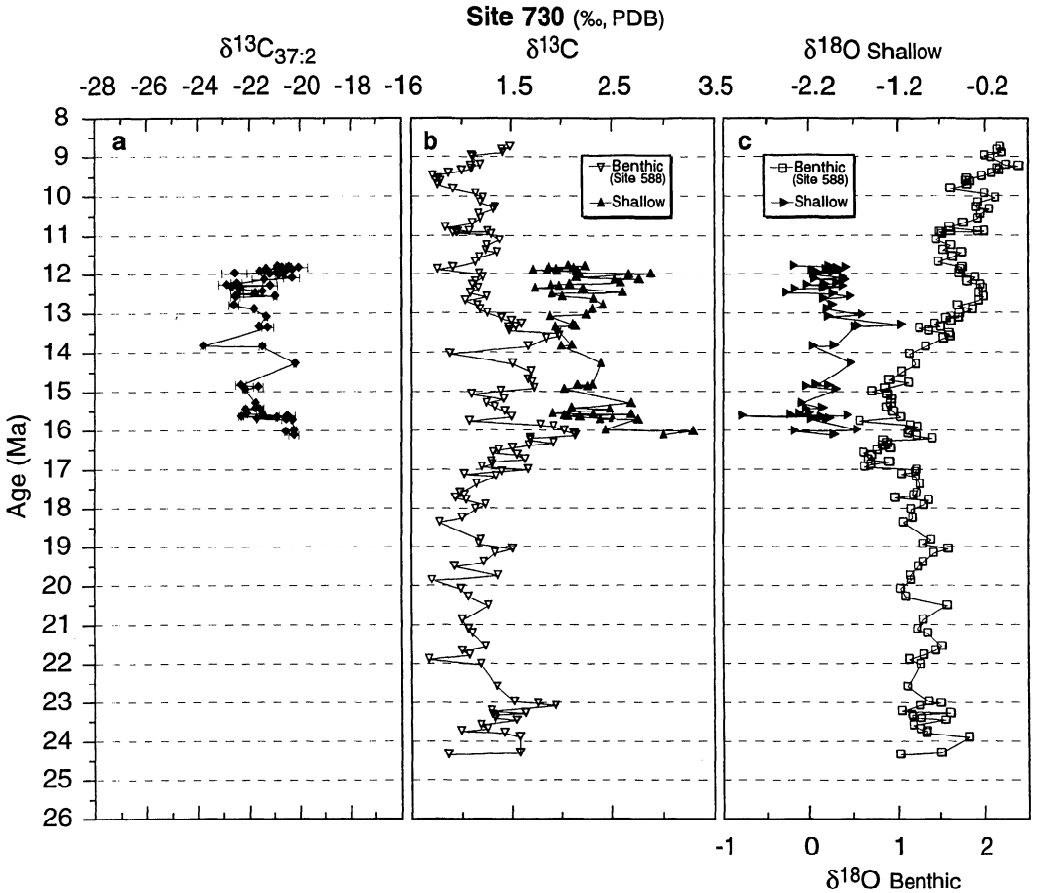

Figure 7. Total isotope data from site 730. See Figure 5 caption for details. Data for benthic foraminifera are from site 588 [*Kennett*, 1985].

surface water [$CO_{2(aq)}$] were limiting to algal growth, then lower CO_2 (i.e., during Pleistocene glacial intervals as well as calculated Miocene levels) would necessitate a carbon concentrating mechanism (CCM) to be operational during photosynthesis. Although for many organisms this is likely the case, for the extant *E. huxleyi* this is difficult to imagine because no such physiological mechanism is recognized. The evolution and dominance of *E. huxleyi* in the world's oceans during the Pleistocene and Holocene [*Hay*, 1977] implies that the low CO_2 concentrations and apparent lack of a CCM during glacial intervals did not significantly impair their ecological advantage. The consistency of Miocene $\varepsilon_{p37:2}$ values from the three widely distributed sites of this study continues to argue for similar processes occurring in a global context.

If Miocene low $\varepsilon_{p37:2}$ values resulted because a CCM was operational, it implies carbon limitation in oligotrophic environments. Although this would result in an underestimation of pCO_2 and prevent accurate calculations of atmospheric pCO_2, it would still support our overall conclusions for low concentrations of surface water and atmospheric CO_2. Therefore, until evidence emerges to the contrary we assume that the physical and physiological processes responsible for the isotopic character of $C_{37:2}$ alkenones from the Miocene are similar to those operating in modern surface waters.

Other sources of error, such as a possible decoupling between micronutrient and phosphate concentrations or differences in the *b* versus [PO_4^{3-}] relationship during the Miocene, are difficult to assess. It is important to note that the level of phosphate in the modern ocean does not limit haptophyte growth rates. *Bidigare et al.* [1997] suggest that the *b* versus [PO_4^{3-}] relationship (Figure 4b) is driven by variation in growth-rate-limiting micronutrients that covary with [PO_4^{3-}]. Because it is unknown which micronutrient(s) (i.e., Zn, Co, Fe, etc.) is (are) limiting haptophyte growth in the modern ocean, it is impossible to surmise how the relationship between ε_p and [PO_4^{3-}] may have been different in ancient oceans. Furthermore, little is known about the history of micronutrient inventories. *Delaney* [1990] argued that the Miocene Cd reservoir appears ~20% lower than that recorded for the Quaternary. If we were to assume a worse case scenario, i.e., Cd and other micronutrients ($Cd_{nutrients}$) were decoupled from [PO_4^{3-}] such that the $Cd_{nutrients}$/[PO_4^{3-}] ratio was lower during this time, then Miocene pCO_2 could potentially be underestimated by 20%.

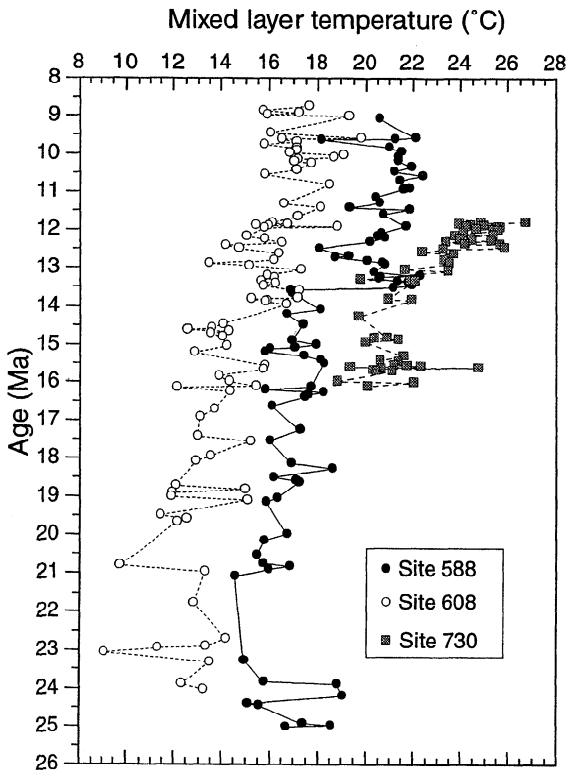

Figure 8. Mixed layer temperatures calculated from the $\delta^{18}O$ of shallow-dwelling planktonic foraminifera. Calibration of *Erez and Luz* [1983] was applied. A value of -1‰ (SMOW) is assumed for δw prior to East Antarctic ice sheet (EAIS) expansion. Changes in δw (see Figure 1) follow the conclusions of *Flower and Kennett* [1993].

Popp et al. [1998a] have demonstrated a direct relationship between ε_p and cell volume to surface area ratio. In the modern ocean, alkenone-producing haptophytes have a spherical geometry, thus changes in cell diameter minimize changes in volume to surface area compared to other cell geometries [*Popp et al.*, 1998a]. Measured cell diameters of *E. huxleyi* kept in culture at the Provasoli-Guillard National Center for Culture of Marine Phytoplankton [http://ccmp.bigelow.org] are predominantly in the range of 3 to 6 μm, corresponding to approximately 30% uncertainty in calculated $[CO_{2(aq)}]$ (*B.N. Popp*, personal communication, 1998). If open ocean Miocene haptophytes averaged larger cell diameters, an argument unsubstantiated by available research, then our estimates would represent an underestimation of Miocene pCO_2. However, error analyses for both micronutrient inventories and cell geometries are highly speculative. Although the above arguments add uncertainty into our final pCO_2 estimates, they represent extreme case scenarios and should be considered as such.

Finally, an additional source of error, addressed in a previous section, concerns the reliability of foraminiferal isotopic compositions. Carbonate diagenesis would affect both the absolute expression of $\varepsilon_{p37:2}$ and our estimates of pCO_2. Diagenetic processes such as differential dissolution, reprecipitation, and carbonate infilling would tend to enrich foraminiferal $\delta^{18}O$ compositions, register lower isotopic temperatures, and lead to an underestimation of pCO_2. However, given that calculated $[CO_{2(aq)}]$ are low, temperature estimates would have to be significantly in error to greatly affect pCO_2 estimates (Figure 12). For example, a lowering of surface water temperatures from 20° to 16°C (corresponding to an ~+1‰ change in

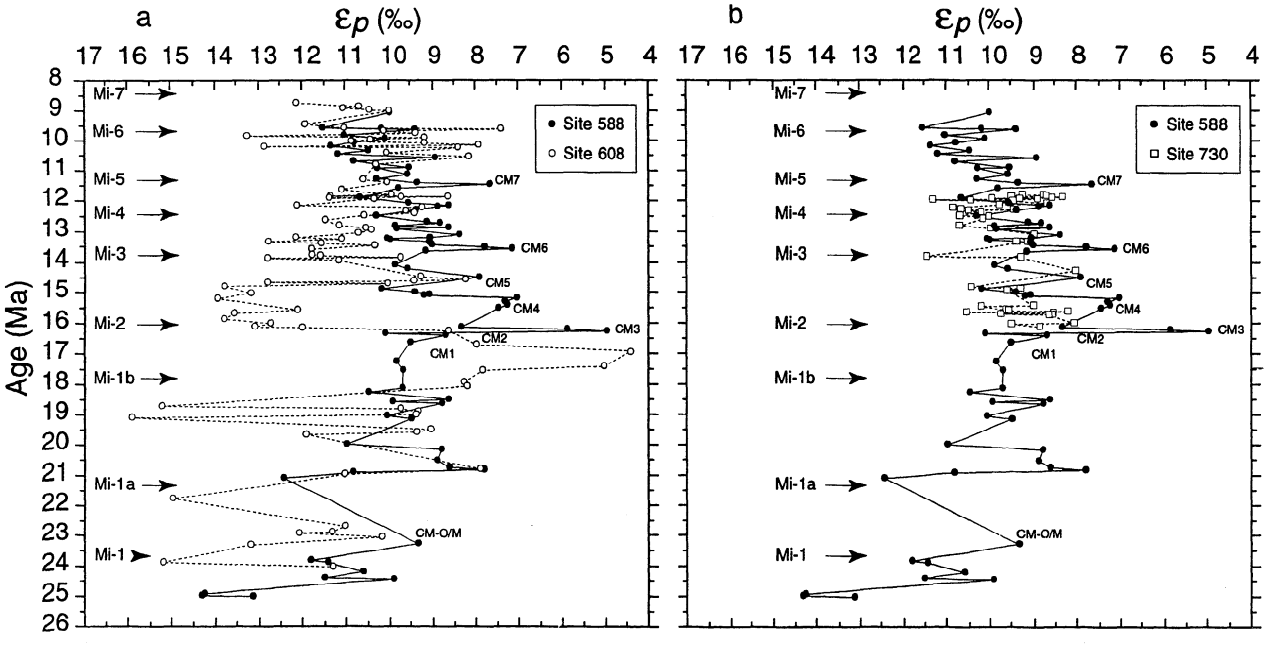

Figure 9. (a) Comparison of ε_p trends from sites 588 (solid circles) and 608 (open circles). (b) Comparison of ε_p trends from sites 588 (solid circles) and 730 (open squares). CM's represent the carbon maxima events of *Woodruff and Savin* [1991]. Mi events represent inferred glacial maximums [*Miller et al.*, 1987; *Wright et al.*, 1992].

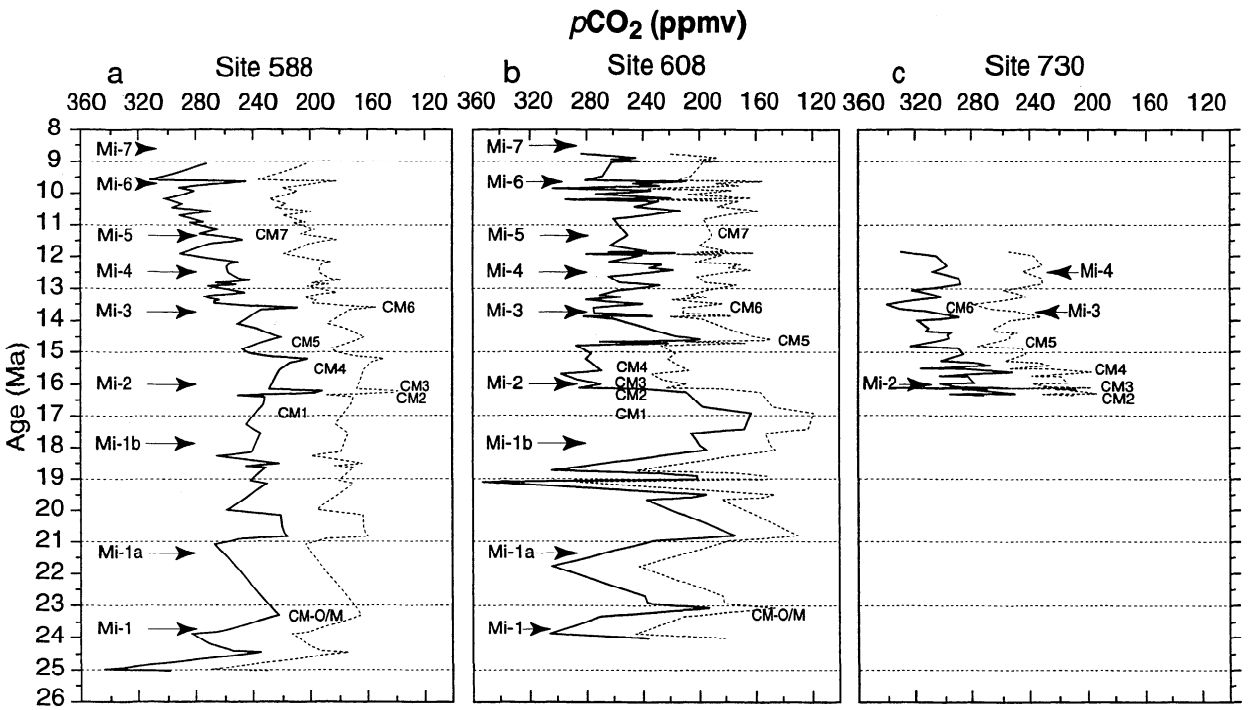

Figure 10. Maximum and minimum pCO_2 estimates using equations from Table 2. The thick lines represent maximum pCO_2 values calculated using the equation for the maximum 95% confidence interval, $[PO_4]$ = 0.3 μM, and ε_f = 27‰. The thin lines represent minimum pCO_2 values calculated using the equation for the minimum 95% confidence interval, $[PO_4]$ = 0.2 μM, and ε_f = 25‰. CM and Mi are carbon maxima events and inferred glacial maximums, respectively.

foraminiferal $\delta^{18}O$) would result in a ~30 ppmv lowering of pCO_2 in equilibrium with water containing 10 μmol kg^{-1} of $CO_{2(aq)}$. Although quantification of carbonate diagenesis was not an objective of this study, consistent temporal alteration of texturally well-preserved foraminifera tests is not likely

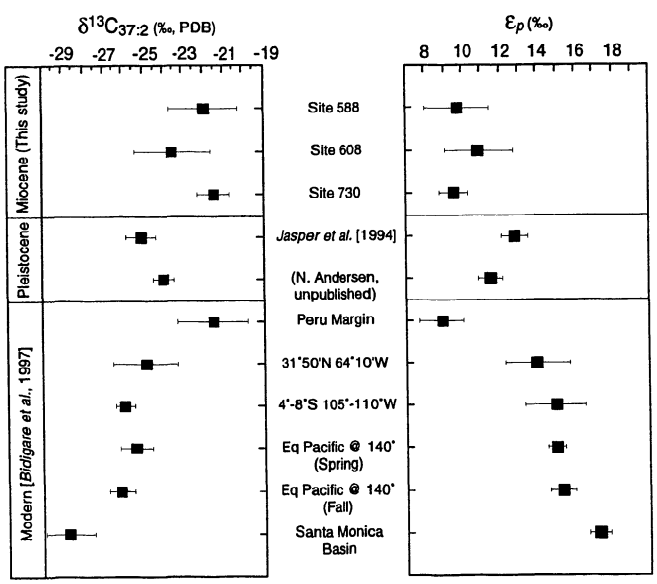

Figure 11. Compilation of published $\delta^{13}C_{37:2}$ and $\varepsilon_{p37:2}$ data.

[*Miller et al.*, 1987]. We conclude on the basis of visual examination and preservation of characteristic $\delta^{13}C$ and $\delta^{18}O$ trends and events that carbonate diagenesis contributed little to the expression of pCO_2 trends during the Miocene.

Possible fluctuations of 1.0-0.5‰ in δw related to ice volume variation have been proposed for several Miocene glacial episodes [*Miller et al.*, 1991; *Wright et al.*, 1992]. As noted above, changes of this magnitude, as they affect surface water temperature estimates, would not greatly alter calculated pCO_2 trends, although they may enhance the relationship between pCO_2 and glacial intervals. Allowing a linear increase and decrease of 0.5‰ across glacial episodes Mi1, Mi1a, Mi1b, and Mi2 (Figure 13), maximum pCO_2 is recalculated (Figure 14). In accordance with our assessment of paleoceanography (discussed below), we assume the record from site 588 is representative of global trends and compare it against inferred episodes of increased organic burial, glaciation, and silicate chemical weathering.

Propagation of errors was determined using a Monte Carlo procedure. We assume uncertainties in our method include $[PO_4^{3-}]$ ±0.1, T°C ±2, salinity ±1, ε_f ±1, analytical errors for $\delta_{37:2}$ and $\delta^{13}C_{carb}$ of ±0.5‰ and ±0.2‰, respectively, and an 11% uncertainty about the slope and intercept of the b versus $[PO_4]$ geometric mean regression (representing the 95% confidence interval). Our simulation results in a 15% uncertainty for calculated pCO_2 values. Therefore we conclude that our pCO_2 estimates are robust given all known and reasonable uncertainties.

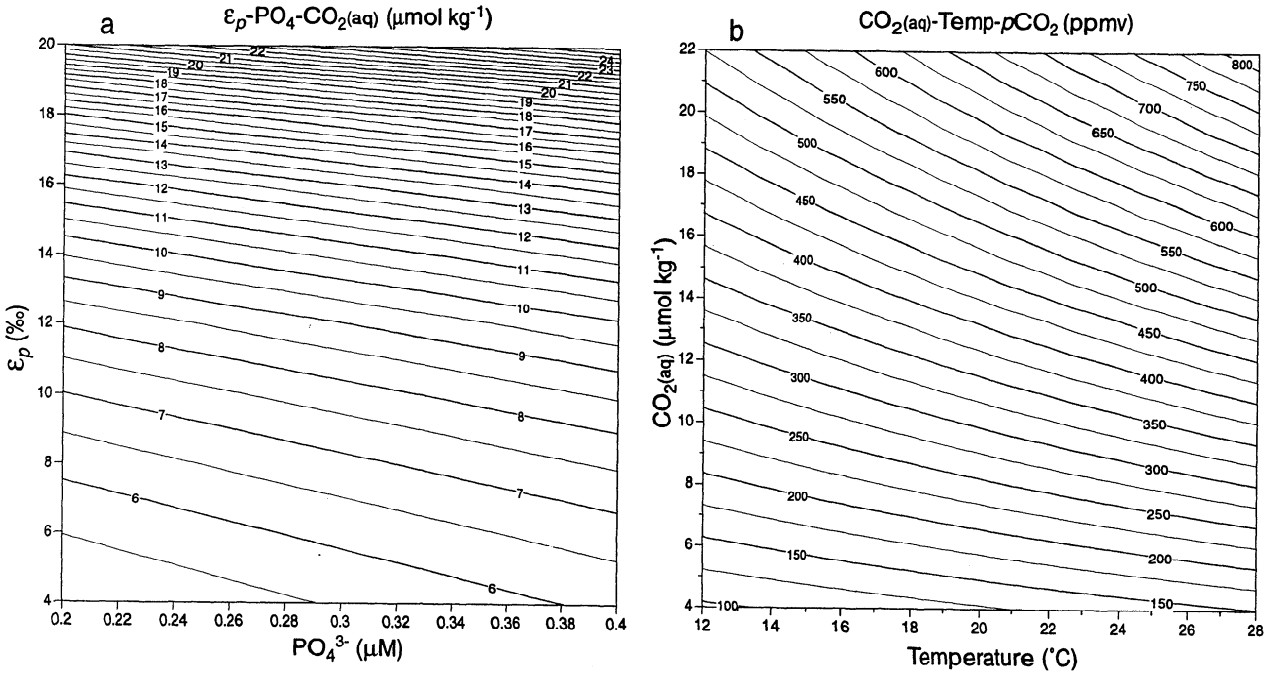

Figure 12. (a) $CO_{2(aq)}$ as a function of $[PO_4]$ and ε_p. $CO_{2(aq)}$ is calculated using the equation for the geometric regression generated using data of *Bidigare et al.* [1997, 1999] and *B.N. Popp*, (unpublished data, 1999), with $\varepsilon_f = 27‰$. (b) pCO_2 as a function of temperature and $CO_{2(aq)}$.

6.2. Apparent pCO_2 Differences Between Ocean Basins

The overall similarities in $\varepsilon_{p37:2}$ measured from all three sites have significant implications concerning the role of pCO_2 during climate change in the Miocene (discussed below). However, an equally important contribution is understanding the differences in the isotopic trends between sites. Because $\varepsilon_{p37:2}$ varies inversely with surface water $[CO_{2(aq)}]$ and directly with haptophyte growth rates, changes in water chemistry, ocean-atmosphere gas equilibrium, physical oceanographic conditions, and thermocline strength can result in spatial variations in the expression of $\varepsilon_{p37:2}$ trends through time.

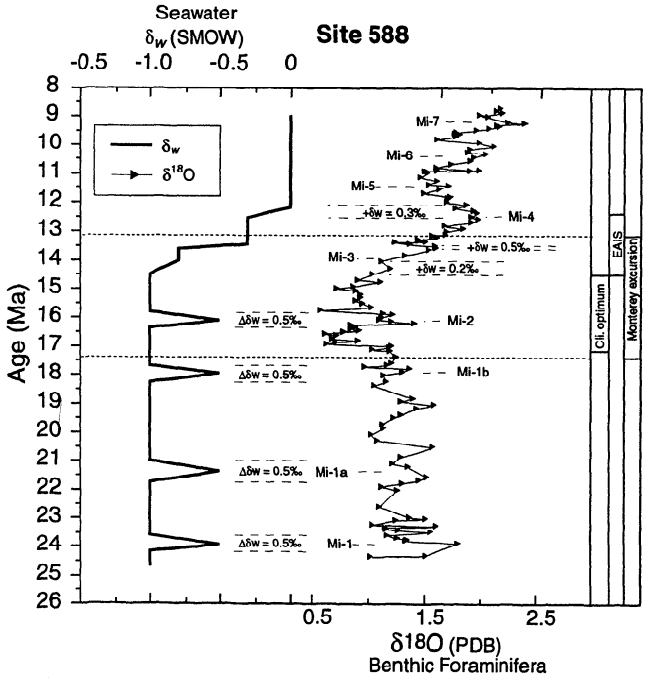

Figure 13. Schematic representation of changes in δw used to calculate sea surface temperatures and pCO_2. A linear 0.5‰ increase and decrease in δw are assumed across glacial episodes Mi1, Mi1a, Mi1b, and Mi2. Cli. optimum is climatic optimum.

Available data provide evidence that changes in circulation patterns through time affected photic-zone properties at site 608. Dramatic variations in deep and intermediate water circulation occurred involving the strength and presence of northern component waters (NCW) and southern component waters (SCW) [*Woodruff and Savin*, 1989; *Wright et al.*, 1992]. Deep water formation appears to have oscillated between North Atlantic and Southern Ocean sources with NCW dominance between ~20-15 Ma (reaching peak production by ~17 Ma) and ~12.5-8.5 Ma and SCW dominance between ~25-20 and 15-12.5 Ma [*Wright et al.*, 1991, 1992; *Wright and Miller*, 1996].

Changes in deep and surface circulation had the potential to significantly alter the climatic and oceanographic character of the North Atlantic region. For example, in an assessment of the timing and relative influence of NCW throughout the Neogene, *Wright and Miller* [1996] conclude that variation in NCW production is correlative with changes in global and regional climates during the middle Miocene and Pliocene. Specifically, the period of global warmth between 17 and 16 Ma is associated with peak production of NCW. High NCW outflux would be compensated by increased influx of warm surface water, increasing the transport of heat and moisture to the North Atlantic and potentially maintaining an ice-free Arctic Ocean [*Wright and Miller*, 1996]. This interpretation

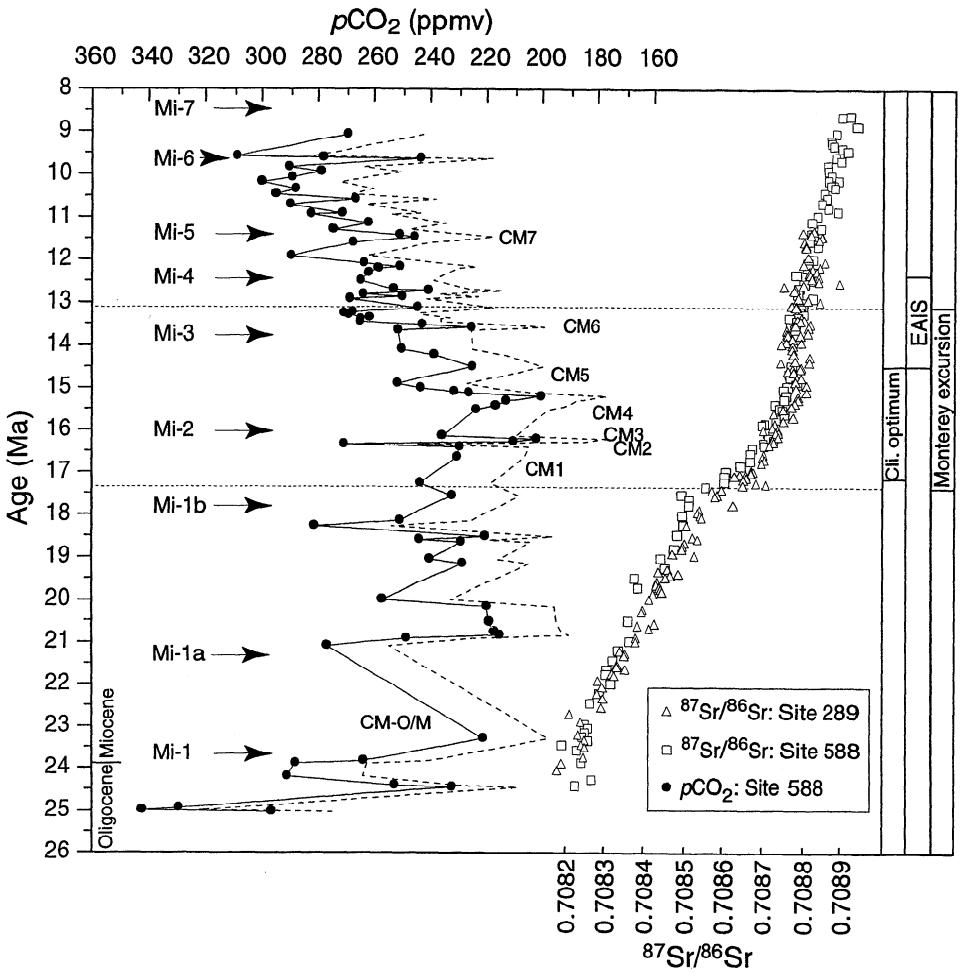

Figure 14. Maximum pCO_2 estimates (solid circles) using ε_p values from site 588, the equation for the maximum 95% confidence interval (Table 2), a $[PO_4]$ of 0.3 μM, and $\varepsilon_f = 27‰$. CM and Mi represent carbon maximas and inferred glacial maximums. A linear 0.5‰ increase and decrease in δw are assumed across glacial episodes Mi1, Mi1a, Mi1b, and Mi2 in addition to permanent δw changes during EAIS expansion (see Figure 13). Data for Sr isotope ratios are from sites 588 (open squares) and 289 (open triangles) from *Hodell et al.* [1991] and *Hodell and Woodruff* [1994]. Cli. optimum is climatic optimum. Note that the dashed line was calculated using the equation of the geometric mean regression (Table 2) and assuming $\varepsilon_f = 25‰$. Propagation of error described in text results in a 15% uncertainty about calculated pCO_2 estimates.

is supported by biogeographical distributions of tropical-subtropical and transitional assemblages of planktonic foraminifera in the North Atlantic. In general, these assemblages expanded and contracted during the early to late Miocene in response to changing surface water characteristics [*Thunell and Belyea,* 1982]. Specifically, warm surface waters extended into high northern latitudes during the early Miocene (~22.5-17.5 Ma) possibly driven by current systems similar to the modern gulf stream. During the middle Miocene (~13.5 Ma) the development of a cool North Atlantic eastern boundary current coincides with the contraction of the tropical-subtropical province to lower latitudes [*Thunell and Belyea,* 1982].

Stable isotope analyses of surface- and deep-dwelling planktonic foraminifera from site 608 reveal rapid and large-scale oscillations (~0.8-1.0‰) in surface to thermocline $\delta^{18}O$ gradients ($\Delta\delta^{18}O$) throughout the early to middle Miocene [*Pagani,* 1998]. The waxing and waning of thermocline strength, implied by variable $\Delta\delta^{18}O$, were likely associated with variations in surface water $[CO_{2(aq)}]$ and nutrient budgets. Furthermore, diatomaceous sediments, indicative of higher nutrient supply to surface waters and/or decreased bottom water corrosivity to opal, occur between ~13.3-12 Ma at site 608 [*Baldauf,* 1987; *Westerberg-Smith,* 1987], with initiation of a two-fold increase in the apparent sedimentation rate coinciding with opal enrichment and continuing to 9 Ma (Figure 3).

Distinctive changes in North Atlantic benthic foraminifer abundances [*Belanger and Berggren,* 1986] and faunal compositions [*Schnitker,* 1986; *Thomas,* 1986] occur in the early to middle Miocene influenced by the strength of NCW and high-latitude cyrospheric evolution. Notably, the appearance of *Bolivina* spp. is unusual at site 608 (~19-16.5 Ma with peak abundances between ~17.5 and 16.8 Ma) [*Thomas,* 1986]. This benthic foraminifer is ascribed to low-oxygen, high organic carbon environments [*Boltovskoy and Wright,* 1976] with high faunal abundances found in shelf-slope areas

underlying highly productive surface waters. The occurrence of *Bolivina* spp. has not been adequately explained. It is curious that a major decrease in $\varepsilon_{p37:2}$ values between ~17.5-16.7 Ma appears to occur coincident with the appearance and dominance of *Bolivina* spp. at site 608. Integration of these biological and geochemical proxies leads us to suggest that increased phytoplanktic growth rates and export productivity resulted in decreased bottom water dissolved oxygen concentrations. Higher growth rates would lead to lower $\varepsilon_{p37:2}$ values and explain both the organic and inorganic isotopic trends observed during this time.

In contrast to site 608, the surface-water temperature at site 588 appears quite stable with consistent $\Delta\delta^{18}O$ values between near surface and thermocline waters (~0.5‰) during the early to middle Miocene [*Flower and Kennett,* 1993; this study]. Only minor changes in benthic foraminiferal assemblages related to the middle Miocene cooling event occurred in this region [*Kurihara and Kennett,* 1992]. Low, steady sedimentation rates and a consistent sedimentological character imply relative oceanographic stability. A 3°-4°C warming of surface waters occurred at ~13.5 Ma and is potentially related to the strengthening of the East Australia Current [*Flower and Kennett,* 1993]; however, significant ecological changes are not evident. Therefore the available evidence suggests that the $\varepsilon_{p37:2}$ record from site 608 has been overprinted by regional processes while site 588 is more representative of global CO_2 trends.

Alkenone abundances are much greater at site 730 than at sites 588 and 608 [*Pagani,* 1998]. This implies that haptophyte productivity was higher in the northern Arabian Sea. At present the Oman margin is characterized by seasonal upwelling caused by monsoonal atmospheric circulation patterns (see *Emeis et al.,* [1995] for a review). Responding to the increased nutrient flux to surface waters, rates of primary productivity are quite high, ranging from >2.5 gC m^{-2} d^{-1} in marginal waters to <0.3 gC m^{-2} d^{-1} in waters outside the upwelling region [*Owens et al.,* 1993]. Initiation of monsoon-driven upwelling in the northern Indian Ocean is estimated to have begun in the late Miocene (~11.9-8.5 Ma) on the basis of the appearance of indicators such as diatomaceous sediments [*Burckle,* 1989; *Nigrini,* 1991] and *Globigerina bulloides* [*Kroon et al.,* 1991]. If haptophyte growth rates were higher at site 730 relative to site 588, then the occurrence of similar ε_p values during the middle Miocene (Figure 9b) requires higher surface water $[CO_{2(aq)}]$ at site 730 during this time.

A positive correlation between CM events and decreases in estimated pCO_2 suggests that increases in the burial flux of organic carbon impacted carbon dioxide concentrations on ~400 kyr timescales [*Woodruff and Savin,* 1991]. In addition, this relationship lends support to the hypothesis that changes in high-latitude temperatures and/or ice growth was promoted and /or accompanied by changes in the rate of organic carbon burial. However, because some glacial episodes do not have a correlative CM event (Mi1a, Mi1b, Mi4, Mi6, and Mi7), organic burial cannot be the sole factor driving short-term high-latitude cooling throughout the Miocene.

6.3. Changes in pCO_2 During Inferred Glaciations

In general, decreases of <40 ppmv are associated with inferred glacial episodes as defined by *Miller et al.,* [1987]. The largest and most abrupt decrease in pCO_2 occurs at ~25 Ma. Within ~400 kyr, pCO_2 concentrations decline from ~350 to 220 ppmv. An increase to previous levels followed by a fall at 23.9 Ma, near the Oligocene/Miocene boundary, marks the return of the pCO_2 concentration to ~220-200 ppmv. The timing of this pCO_2 decrease coincides with the development of glacial episode Mi1, which was recently characterized as a well-developed glacial interval with Milankovitch periodicities [*Zachos et al.,* 1997]. Further, an ~1.2‰ enrichment in benthic $\delta^{18}O$ records from the equatorial Atlantic [*Zachos et al.,* 1997], coupled with an inferred glacioeustatic sea level lowering [*Miller and Sugarman,* 1995] suggests that significant continental ice accumulation occurred during this time. Following Mi1, it appears that a new steady state pCO_2 concentration is established. The remainder of the early and middle Miocene is characterized by relatively low CO_2 concentrations (~260-190 ppmv), in accordance with evidence of episodic glaciation throughout this period. The intervals of lowest pCO_2 occur at ~16 and 15.3 Ma within the Monterey excursion (CM3 and CM4, respectively). Atmospheric carbon dioxide rises following the expansion of EAIS to concentrations approaching Pleistocene interglacial levels.

During the Pleistocene, minor alterations in ocean circulation, driven by orbitally controlled changes in insolation, have been implicated as the trigger of glacial/interglacial variation [*Broecker et al.,* 1985; *Boyle,* 1988; *Broecker and Peng,* 1989]. Given the low and similar concentrations of pCO_2 for both the Miocene and Pleistocene, one would expect the Miocene climate system to have been similarly sensitive to changes in heat and vapor transport. Perhaps the causes of transitory Miocene glaciation and pCO_2 variability are comparable to those for the Pleistocene.

7. Implications

The use of the strontium isotope record as a monitor of silicate chemical weathering rates [*Kump,* 1989; *Raymo,* 1991; *Palmer and Edmond,* 1992; *Kump and Arthur,* 1997] and the timing of major Himalayan uplift and erosion [*Rea,* 1992] are topics of strong debate. Nevertheless, if the Sr isotope record is a strict proxy for chemical weathering rates, then one would anticipate a continuous decline of pCO_2 throughout the Miocene if the rate of magmatic CO_2 influx remained constant, and other compensatory effects (e.g., decrease in organic carbon burial) were not significant. Moreover, the greatest rate of change in the Sr isotope record demands that the most rapid rates of carbon dioxide removal occurred between ~21 and 17 Ma [*Hodell and Woodruff,* 1994]. However, this removal is not observed in our results. Instead, following the expansion of the EAIS in the middle Miocene, we find that pCO_2 steadily increased. The rise of pCO_2 following the expansion of the EAIS has two possible explanations (assuming long-term volcanic CO_2 input has remained constant). First, a negative trend in the inorganic $\delta^{13}C$ record through the middle and late Miocene calls for additional inputs of CO_2 via a reduction in organic carbon burial [*Shackleton,* 1987] and/or reoxidation of organic carbon deposited on shelves as the result of falling sea levels [*Vincent and Berger,* 1985]. A negative shift of 1‰ at ~13.5 Ma marks the return of inorganic $\delta^{13}C$ values to pre-"Monterey" event values. This implies that the amount of CO_2 returned to the atmosphere following EAIS expansion was

equivalent to that removed during the Monterey $\delta^{13}C$ excursion and is associated with an ~30 ppmv rise in pCO_2 (Figure 14). However, our record shows that an additional ~60 ppmv rise occurred between 14 and 10 Ma.

Our preferred explanation calls for reductions in silicate chemical weathering and a subsequent pCO_2 rise as the result of falling high-latitude temperatures and regional ice coverage on Antarctica. This scenario and our pCO_2 estimates are supported by recent geochemical modeling of carbon and strontium cycles during the Cenozoic [*Kump and Arthur,* 1997]. As a corollary, the lack of an appreciable ice sheet in the late early Miocene with a correspondingly lower global albedo could have allowed a more equable latitudinal temperature gradient to develop during a period of relatively low pCO_2. Thus we suggest that the climatic optimum of the late early Miocene could develop under low pCO_2 conditions because of the absence of a large polar ice sheet.

In summary, the lack of a correspondence between Sr and pCO_2 argues against the use of the Sr isotope record as a proxy for global chemical weathering rates during this time. This does not negate the possibility that slight imbalances between silicate weathering rates and CO_2 inputs generated declines in pCO_2 during other times in the Cenozoic.

Perhaps the most dramatic observation of this study is the overall uniformly low pCO_2 level recorded from all three cores (Figure 10). The early to late Miocene pCO_2 concentrations estimated from our data are similar to those recorded for Pleistocene interglacial-glacial intervals, with maximum calculated pCO_2 values of ~290 ppmv. The noticeable absence of large-scale changes in pCO_2 at site 588 following the ~100 ppmv decrease in the early Miocene appears in conflict with greenhouse theories of climate change. In particular, there is no evidence for a sharp decline in pCO_2 associated with EAIS expansion, or a rise in pCO_2 during the late early Miocene "climatic optimum." Nevertheless, critically low levels of pCO_2, capable of forcing EAIS expansion, could have been approached if (1) concentrations of limiting nutrients were lower than assumed (see Figure 12) or (2) the b versus $[PO_4^{3-}]$ relationship for the modern ocean was different during the middle Miocene. However, lower carbon dioxide concentrations than those estimated (Figure 14) could potentially limit the growth of terrestrial flora [*Lovelock and Whitfield,* 1982; *Sage,* 1995] during the middle Miocene. Regardless, even if limiting nutrients were lower than estimated during the Monterey excursion, the lowest levels of carbon dioxide would still have been achieved ~1 m.y. prior to the expansion of the EAIS. Therefore our results suggest that the late early Miocene climatic optimum and the EAIS expansion in the middle Miocene were not the direct result of large-scale changes in pCO_2, although low pCO_2 estimated for this time could have allowed the climate system to respond sensitively to changes in heat and water vapor transport. Consequently, we emphasize an oceanographic control on Miocene climate change.

For example, the opening of the Drake Passage between South America and the Antarctic Peninsula had a profound effect on Southern Ocean circulation, productivity, and the thermal history of Antarctica [*Kennett,* 1977]. As the Drake Passage widened, formation of the Antarctic Circumpolar Current (ACC) would have acted to decouple warm subtropical gyres from Subantarctic and Antarctic gyres, preventing meridional heat transport south of the Antarctic Convergence and thermally isolating Antarctica [*Savin et al.,* 1975; *Barker and Burell,* 1982]. The historical development of the Drake Passage is poorly understood and currently under debate [*Barker and Burell,* 1977; *Lawver and Gahagan,* 1998]. However, *Barker and Burell* [1977, 1982], on the basis of geophysical and sedimentological data, estimate seafloor spreading in the Drake Passage to have begun ~26 Ma with the subsequent production of deep water flow by ~22 Ma (relative to *Cande and Kent* [1992] ages). Unrestricted flow was potentially delayed until the middle Miocene because of obstructive arrangements of continental fragments and a proto-South Sandwich Island arc in the central Scotia Sea [*Barker and Burell,* 1982; *Barker et al,* 1984].

Carbon and oxygen isotope records of benthic foraminifera in the southwest Pacific Ocean identify periods of intensified Southern Component deep water production between 15.6-13.8 and ~13.8 to 12 Ma [*Flower and Kennett,* 1995]. Moreover, distribution and evolution of clay assemblages evaluated from the Weddell Sea mark a transition during the middle Miocene in which physical weathering was favored over chemical weathering, ocean oxidizing conditions increased, and the supply of terrigenous detritus from both South America and west Antarctica was isolated [*Roberts and Maillot,* 1990]. This transition is coincident with a major ice volume increase in East Antarctica and supports a model calling for the development of unrestricted flow through the Drake Passage by ~15 Ma [*Roberts and Maillot,* 1990]. Major changes in meridional heat transport at ~14.5 Ma are further corroborated by a general increase in low-latitude sea surface temperatures coeval with high-latitude cooling [*Savin et al.,* 1985; *Flower and Kennett,* 1993].

8. Conclusions

On the basis of $\varepsilon_{p37:2}$ records derived from three globally distributed oligotrophic sites, we conclude that pCO_2 during the early to late Miocene (25-9 Ma) was similar to levels recorded for Pleistocene glacial/interglacial intervals (290-180 ppmv). The pCO_2 estimates from site 588 record a ~100 ppmv decrease (350-220 ppmv) coincident with a well-defined glacial maximum near the Oligocene/Miocene boundary (Mil of *Miller et al.* [1987]). However, during most of the early to middle Miocene concentrations ranged between 260 and 190 ppmv.

Regardless of the exact magnitude of estimated pCO_2 values, our alkenone isotopic records from three sites consistently indicate that pCO_2 was low throughout the Miocene. Furthermore, although specific trends differ for these three sites, they all lack evidence for either high pCO_2 during the late early Miocene climatic optimum or a sharp decline associated with EAIS growth. The available data suggest that pCO_2 variability played a secondary role in forcing climate change during the Miocene. Instead, it is more probable that tectonic and physical oceanographic factors, including the development of unimpeded flow of the Antarctic Circumpolar Current through the Drake Passage and Scotia Sea and the restriction/cessation of flow across the Indian Ocean and eastern Tethys, exerted dominant control over the development of the early Miocene climatic optimum and expansion of the EAIS. As ice sheets expanded, the resulting increase in albedo enhanced regional and global cooling. The lack of an appreciable ice sheet in the

early Miocene with a correspondingly lower global albedo may have promoted the development of equable latitudinal temperature gradients under low pCO_2. However, low pCO_2 acted to prime the climate system to respond dramatically to changes in oceanography and ice albedo. Furthermore, the long-term increase in pCO_2 following EAIS growth may have been driven by a reduction in chemical weathering rates due to global cooling and regional ice coverage on Antarctica. If this is valid, it suggests that expansion of a continental ice sheet in the Southern Hemisphere directly exerted control on carbon cycling and allowed a higher threshold pCO_2.

Acknowledgments. We would like to thank B. Popp, M. Raymo, and T. Crowley for their critical reviews. Conversations with B. Popp helped to improve the manuscript. Special thanks to D. Walizer, R. Burfield, and G. Montemurro for all their invaluable help in processing samples. Samples for this project were provided by DSDP/ODP. This research was funded by grants from NSF and JOI/USSAC.

References

Baldauf, J. G., Diatom biostratigraphy of the North Atlantic Ocean, Deep Sea Drilling Project Leg 94, *Initial Rep. Deep Sea Drill. Proj., 2*, 729-762, 1987.

Barker, P. F., and J. Burrell, The opening of the Drake Passage, *Mar. Geol., 25*, 15-34, 1977.

Barker, P. F., and J. Burrell, The influence upon Southern Ocean circulation, sedimentation and climate change of the opening of Drake Passage, in *Antarctic Geoscience*, edited by C. Craddock, 377-385, Univ. of Wis. Press, Madison, 1982.

Barker, P. F., P. L. Barber and E. C. King, An early Miocene ridge crest-trench collision on the South Scotia ridge near 36°W, *Tectonophys.,102*, 315-332, 1984.

Bartek, L. R., P. R. Vail, J. B. Anderson, P. A. Emmet, and S. Wu, Effect of Cenozoic ice sheet fluctuations in Antarctica on the stratigraphic signature of the Neogene, *J. Geophy. Res., 96*, 6753-6778, 1991.

Barton, C. E., and J. Bloemendal, Paleomagnetism of sediments collected during Leg 90, southwest Pacific, *Initial Rep. Deep Sea Drill. Proj., 90*, 1273-1316, 1986.

Belanger, P. E., and W. A. Berggren, Neogene benthic foraminifera of the Hatton-Rockall Basin, *Micropaleontology, 32*, 324-356, 1986.

Berggren, W. A., D. V. Kent, and J. A. Van Couvering, Neogene geochronology and chronostratigraphy, in The Chronology of the Geological Record, edited by N. J. Snelling, Geological Society of London Memoir 10, 211-260, 1985.

Berggren, W. A., D. V. Kent, C. C. I. Swisher, and M. P. Aubry, A revised Cenozoic geochronology and chronostratigraphy, in *Geochronology, Time Scales and Global Stratigraphic Correlation*, edited by W. A. Berggren et al., *Spec. Publ. 54*, 129-212, *Soc. of Sed. Geol.*, Tulsa, Okla., 1995.

Bidigare R.R. et al., Consistent fractionation of ^{13}C in nature and in the laboratory: Growth-rate effects in some haptophyte algae, *Global Biogeochem. Cycles, 11*, 279-292, 1997.

Bidigare R.R. et al., Correction to "Consistent fractionation of ^{13}C in nature and in the laboratory: Growth-rate effects in some haptophyte algae" by Bidigare et al., 1997, *Global Biogeochem. Cycles*, in press, 1999.

Bijima, J., Temperature and salinity limits for growth and survival of some planktonic foraminifers in laboratory cultures, *J. Foraminiferal Res., 20*, 95-116, 1990.

Boltovskoy, E., and R. Wright, *Recent Foraminifera*, Stanford, The Hague, Netherlands, 1976.

Boyle, E. A., The role of vertical fractionation in controlling late Quaternary atmospheric carbon dioxide, *J. Geophy. Res., 93*, 15,701-15,714, 1988.

Brassell, S. C., Applications of biomarkers for delineating marine paleoclimatic fluctuations during the Pleistocene, in *Organic Geochemistry: Principles and Application*, edited by M. H. Engel and S. A. Macko, 699-738, Plenum, New York, 1993.

Brassell, S. C., G. Eglinton, I. T. Marlowe, U. Pflaumann, and M. Sarnthein, Molecular stratigraphy: A new tool for climatic assessment, *Nature, 320*, 129-133, 1986.

Broecker, W. S., and T. -H Peng, The cause of the glacial to interglacial atmospheric CO_2 change: A polar alkalinity hypothesis, *Global Biogeochem. Cycles, 3*, 215-239, 1989.

Broecker, W. S., D. M. Peteet, and D. Rind, Does the ocean-atmosphere system have more than one stable mode of operation?, *Nature, 315*, 21-26, 1985.

Burckle, L. H., Distribution of diatoms in sediments of the northern Indian Ocean: Relationship to physical oceanography, *Mar. Micropaleontol., 15*, 53-65, 1989.

Burns, B. D., and J. Beardall, Utilization of inorganic carbon by marine microalgae, *J. Exp. Mar. Biol. Ecol., 107*, 75-86, 1988.

Cande, S. C., and D. V. Kent, A new geomagnetic polarity timescale for the Late Cretaceous and Cenozoic, *J. Geophy. Res., 97*, 13,917-13,951, 1992.

Clement, W. F., and B. M. Robinson, The magnetostratigraphy of Leg 94 sediments, *Initial Rep. Deep Sea Drill. Proj., 94*, 635-650, 1986.

Compton, J. S., S. W. Snyder, and D. A. Hodell, Phosphogenesis and weathering of shelf sediments from the southeastern United States: Implications for Miocene $\delta^{13}C$ excursions and global cooling, *Geology, 18*, 1227-1230, 1990.

Conte, M. H., J. K. Volkman, and G. Eglinton, Lipid biomarkers of the Haptophyta, in *The Haptophyte Algae*, edited by J. C. Green, and B. S. C. Leadbeater, 351-377, Clarendon, Oxford, Eng., U.K., 1994.

Cranwell, P. A., G. Eglinton, and N. Robinson, Lipids of aquatic organisms as potential contributors to lacustrine sediments, II, *Org. Geochem., 6*, 513-527, 1987.

Crowley, T. J., and G. R. North, Abrupt climate change and extinction events in Earth history, *Science, 240*, 996-1001, 1988.

Delaney, M. L., Benthic foraminiferal Cd/Ca records: South Atlantic and western equatorial Pacific, *Paleoceanography, 5*,743-760, 1990.

Emeis, K.-C., D. M. Anderson, H. Doose, D. Kroon, and D. Schulz-Bull, Sea-surface temperatures and the history of monsoon upwelling in the northwest Arabian Sea during the last 500,000 years, *Quat. Res., 43*, 355-361, 1995.

Erez, J., and B. Luz, Experimental paleotemperature equation for planktonic foraminifera, *Geochim. Cosmochim. Acta, 47*, 1025-1031, 1983.

Falkowski,, P. G., Species variability in the fractionation of ^{13}C and ^{12}C by marine phytoplankton, *J. Plankton Res., 13*, 21-28, 1991.

Farquhar, G. D., and P. A. Richards, Isotopic composition of plant carbon correlates with water-use efficiency of wheat genotypes, *Aust. J. Plant Physiol., 11*, 539-552, 1984.

Farquhar, G. D., M. H. O'Leary, and J. A. Berry, On the relationship between carbon isotope discrimination and the intercellular carbon dioxide concentration in leaves, *Aust. J. Plant Physiol., 13*, 281-292, 1982.

Flower, B. P., and J. P. Kennett, Middle Miocene ocean-climate transition: High-resolution oxygen and carbon isotopic records from deep sea drilling project site 588A, southwest Pacific, *Paleoceanography, 8*, 811-843, 1993.

Flower, B. P., and J. P. Kennett, Middle Miocene deepwater paleoceanography in the southwest Pacific: Relations with East Antarctic Ice Sheet development, *Paleoceanography, 10*, 1095-1112, 1995.

Francois, R., M. A. Altabet, R. Goericke, D. C. McCorkle, C. Brunet, and A. Poisson, Changes in the $\delta^{13}C$ of surface water particulate organic matter across the subtropical convergence in the SW Indian Ocean, *Global Biogeochem. Cycles, 7*, 627-644, 1993.

Freeman, K. H., and J. M. Hayes, Fractionation of carbon isotopes by phytoplankton and estimates of ancient CO_2 levels, *Global Biogeochem. Cycles, 6*, 185-198, 1992.

Freeman, K. H., C. J. Boreham, R. E. Summons, and J. M. Hayes, The effect of aromatization on the isotopic compositions of hydrocarbons during early diagenesis, *Org. Geochem., 21*, 1037-1049, 1994.

Gartner, S., Miocene nannofossil chronology in the North Atlantic, DSDP Site 608, *Mar. Micropaleontol.., 18*, 307-331, 1992.

Goericke, R., J. P. Montoya, and B. Fry, Physiology of isotope fractionation in algae and cyanobacteria, in *Stable Isotopes in Ecology*, edited by K. Lajtha and B. Michener, 187-221, Blackwell Sci., Cambridge, Mass., 1994.

Hay, W. W., Calcareous Nannofossils, in *Oceanic Micropaleontology*, vol. *2*, edited by A. T. S. Ramsay, 1055-1200, Academic, San Diego, Calif., 1977.

Hayes, J. M., K. H. Freeman, B. N. Popp, and C. H. Homan, Compound-specific isotopic analyses: A novel tool for reconstruction of ancient biogeochemical processes, *Org. Geochem., 16*, 1115-1128, 1990.

Hinga, K. R., M. A. Arthur, M. E. Q. Pilson, and D. Whitaker, Carbon isotope fractionation by marine phytoplankton in culture: The effects of CO_2 concentration, pH, temperature, and species, *Global Biogeochem. Cycles, 8*, 91-102, 1994.

Hodell, D. A., and F. Woodruff, Variations in the strontium isotopic ratio of seawater during the Miocene: Stratigraphic and geochemical implications, *Paleoceanography, 9*, 405-426, 1994.

Hodell, D. A., P. A. Mueller, and J. R. Garrido, Variations in the strontium isotopic composition of seawater during the Neogene, *Geology, 19*, 24-27, 1991.

Hoefs, M. J. L., G. J. M. Versteegh, W. I. C. Rijpstra, J. W. de Leeuw, and J. S. Sinninghe Damstè, Postdepositional oxic degradation of alkenones: Implications for the measurement of palaeo sea surface temperatures, *Paleoceanography, 13*, 42-49, 1998.

Hollander, D. J., and J. A. McKenzie, CO_2 control

on carbon-isotope fractionation during aqueous photosynthesis: A paleo-pCO_2 barometer: *Geology, 19*, 929-932, 1991.

Huang, Y., G. Eglinton, P. Ineson, P. M. Latter, R. Bol and D. D. Harkness, Absence of carbon isotope fractionation of individual *n*-alkanes in a 23-year field decomposition experiment with *Calluna vulgaris*, *Org. Geochem., 26*, 497-501, 1997.

Jasper, J. P., and J. M. Hayes, A carbon isotope record of CO_2 levels during the late Quaternary, *Nature, 347*, 462-464, 1990.

Jasper, J. P., J. M. Hayes, A. C. Mix, and F. G. Prahl, Photosynthetic fractionation of ^{13}C and concentrations of dissolved CO_2 in the central equatorial Pacific during the last 255,000 years, *Paleoceanography, 9*, 781-798, 1994.

Jenkins, D. G. and M. S. Srinivasan, Cenozoic planktonic foraminifera from the equator to the subantarctic of the southwest Pacific, *Initial Rep. Deep Sea Drill. Proj., 90*, 795-834, 1986.

Kennett, J. P., Cenozoic evolution of Antarctic glaciation the circum-Antarctic Ocean and their impact on global paleoceanography, *J. Geophy. Res., 82*, 3843-3860, 1977.

Kennett, J. P., Miocene to early Pliocene oxygen and carbon isotope stratigraphy in the southwest Pacific, Deep Sea Drilling Project Leg 90, *Initial Rep. Deep Sea Drill. Proj., 90*, 1383-1411, 1985.

Kroon, D., T. N. F. Steens, and S. R. Troelstra, Onset of monsoonal related upwelling in the western Arabian Sea as revealed by planktonic foraminifera, *Proc. Ocean Drill. Program, Sci. Results, 117*, 257-263, 1991.

Kump, L. R., Alternative modeling approaches to the geochemical cycles of carbon, sulfur, and strontium, *Am. J. Sci., 289*, 390-410, 1989.

Kump, L. R., and M. A. Arthur, Global chemical erosion during the Cenozoic, in *Tectonic Uplift and Climate Change*, edited by W. F. Ruddiman, 399-426, Plenum, New York, 1997.

Kurihara, K., and J. P. Kennett, Paleoceanographic significance of Neogene benthic foraminifera changes in a southwest Pacific bathyal depth transect, *Mar. Micropaleontol., 19*, 181-199, 1992.

Laws, E. A., B. N. Popp, R. R. Bidigare, M. C. Kennicut, and S. A. Macko, Dependence of phytoplankton carbon isotopic composition on growth rate and $[CO_{2aq}]$: Theoretical considerations and experimental results, *Geochim. Cosmochim. Acta, 59*, 1131-1138, 1995.

Lawver, L. A., and L. M. Gahagan, Opening of the Drake Passage and its impact on Cenozoic ocean circulation, in *Tectonic Boundary Conditions for Climate Reconstructions*, edited by T. J. Crowley and K. C. Burke, 212-223, Oxford Univ. Press, New York, 1998.

Leckrone, K. J., and J. M Hayes, Efficiency and temperature-dependence of water removal by membrane dryers, *Anal. Chem., 69*, 911-918, 1997.

Lovelock, L. E., and M. Whitfield, Life span of the biosphere, *Nature, 296*, 561-563, 1982.

Marlowe, I. T., J. C. Green, A. C. Neal, S. C. Brassell, G. Eglinton, and P. A. Course, Long chain (n-C37-C39) alkenones in the Prymnesiophycea: Distribution of alkenones and other lipids and their taxonomic significance, *Br. Phycol. J., 19*, 203-216, 1984.

McCabe, B., The dynamics of ^{13}C in several New Zealand lakes, Ph.D. dissertation, Univ. of Waikato, Hamilton, N.Z., 1985.

Merritt, D. A., K. H. Freeman, M. P. Ricci, S. S. Studley, and J. M. Hayes, Performance and optimization of a combustion interface for isotope ratio monitoring gas chromatography/mass spectrometry, *Anal. Chem., 67*, 2461-2473, 1995.

Miller, K. G., and P. J. Sugarman, Correlating Miocene sequences in onshore New Jersey boreholes (ODP Leg 150X) with global $\delta^{18}O$ and Maryland outcrops, *Geology, 23*, 747-750, 1995.

Miller, K. G., R. G. Fairbanks, and G. S. Mountain, Tertiary oxygen isotope synthesis, sea level history, and continental margin erosion, *Paleoceanography, 2*, 1-19, 1987.

Miller, K. G., J. D. Wright, and R. G. Fairbanks, Unlocking the ice house: Oligocene-Miocene oxygen isotopes, eustacy, and margin erosion, *J. Geophy. Res., 96*, 6829-6848, 1991.

Mook, W. G., J. C. Bommerson, and W. H. Staberman, Carbon isotope fractionation between dissolved bicarbonate and gaseous carbon dioxide, *Earth Planet. Sci. Lett., 22*, 169-176, 1974.

Nigrini, C., Composition and biostratigraphy of radiolarian assemblages from an area of upwelling (northwestern Arabian Sea, Leg 117), *Proc. Ocean Drill. Program Sci. Results, 117*, 89-126, 1991.

Nimer, N. A., and M. J. Merrett, Calcification and utilization of inorganic carbon by the coccolithophorid *Emiliania huxleyi* Lohmann, *New Phytol., 121*, 173-177, 1992.

Nimer, N. A., G. K. Dixon, and M. J. Merrett, Utilization of inorganic carbon by the coccolithophorid *Emiliania huxleyi* (Lohmann) Kamptner, *New Phytol., 120*, 153-158, 1992.

Nimer, N. A., Q. Guan, and M. J. Merrett, Extra- and intra-cellular carbonic anhydrase in relation to culture strain of *Emiliania huxleyi* Lohmann, *New Phytol., 126*, 601-607, 1994.

Oslick, J. S., K. G. Miller, M. D. Feigenson, and J. D. Wright, Oligocene-Miocene strontium isotopes: Stratigraphic revisions and correlations to an inferred glacioeustatic record, *Paleoceanography, 9*, 427-443, 1994.

Owens, N. J., P. H. Burkill, R. F. C. Mantoura, E. M. S. Woodward, I. A. Bellan, J. Aiken, R. J. M. Howland, and C. A. Llewellyn, Size fractionated primary production and nitrogen assimilation in the NW Indian Ocean, *Deep Sea Res. part II, 40*, 697-709, 1993.

Pagani, M., Miocene atmospheric carbon dioxide concentrations and paleoceanography: Constraints from compound-specific isotope compositions: Ph.D. dissertation, Penn. State Univ., University Park, 1998.

Palmer, M. R., and J. M. Edmond, Controls over the strontium isotope composition of river water, *Geochim. Cosmochim. Acta, 56*, 2099-2111, 1992.

Pekar, P., and K. G. Miller, New Jersey Oligocene "Icehouse" sequences (ODP Leg 150X) correlated with global $\delta^{18}O$ and Exxon eustatic records, *Geology, 24*, 567-570, 1996.

Popp, B. N., E. A. Laws, R. R.Bidigare, J. E. Dore, K. L. Hanson, and S. G. Wakeham, Effect of phytoplankton cell geometry on carbon isotopic fractionation, *Geochim. Cosmochim. Acta, 62*, 69-77, 1998a.

Popp, B. N., F. Kenig, S. G. Wakeham, E. A Laws, R. R. and Bidigare, Does growth rate affect ketone unsaturation and intracellular carbon isotopic variability in *Emiliania huxleyi*?, *Paleoceanography, 13*, 35-41, 1998b.

Prahl, F. G., and S. G. Wakeman, Calibration of unsaturation patterns in long-chain ketone compositions for palaeotemperature assessment, *Nature, 330*, 367-369, 1987.

Quiroga, O., and E. Gonzalez, Carbonic anhydrase in the choloroplast of a coccolithophorid (Prymnesiohycea), *J. Phycol., 29*, 321-324, 1993.

Rau, G. H., T. Takahashi, and D. J. Des Marais, Latitudinal variations in plankton $\delta^{13}C$: implications for CO_2 and productivity in past oceans, *Nature, 341*, 519-518, 1989.

Rau, G. H., P. N. Froelich, T. Takahashi, and D. J. Des Marais, Does sedimentary organic $\delta^{13}C$ record variations in Quaternary ocean $[CO_{2aq}]$?, *Paleoceanography, 6*, 335-347, 1991.

Rau, G. H., T. Takahashi, D. J. Des Marais, D. J. Repeta, and J. H. Martin, J. H., The relationship between $\delta^{13}C$ of organic matter and $[CO_2(aq)]$ in ocean surface water: Data from a JGOFS site in the northeast Atlantic Ocean and a model, *Geochim. Cosmochim. Acta, 56*, 1413-1419, 1992.

Rau, G. H., U. Riebesell, and D. Wolf-Gladrow, A model of photosynthetic ^{13}C fractionation by marine phytoplankton based on diffusive molecular CO_2 uptake, *Mar. Ecol. Prog. Ser., 133*, 275-285, 1996.

Raven, J. A., and A. M. Johnston, A. M., Mechanisms of inorganic-carbon acquisition in marine phytoplankton and their implications for the use of other resources, *Limnol. Oceanogr., 36*, 1701-1714, 1991.

Raymo, M. E., Geochemical evidence supporting T.C. Chamberlin's theory of glaciation, *Geology, 19*, 344-347, 1991.

Raymo, M. E., The Himalayas, organic carbon burial, and climate in the Miocene, *Paleoceanography, 9*, 399-404, 1994.

Rea, E. K., Delivery of Himalayan sediment to the northern Indian Ocean and its relationship to global climate, sea level, uplift, and seawater strontium, in *Synthesis of Results from Scientific Drilling in the Indian Ocean*, *Geophys. Monogr. Ser*, vol. 70, edited by R. Duncan and D. Rea, 387-402, AGU, Washington, D.C., 1992.

Rechka, J. A., and J. R. Maxwell, Characterisation of alkenone temperature indicators in sediments and organisms, *Org. Geochem., 13*, p. 727-734, 1987.

Ricci, M. P., D. A. Merritt, K. H. Freeman, and J. M. Hayes, Acquisition and processing of data for isotope-ratio-monitoring mass spectrometry, *Org. Geochem., 21*, 561-571, 1994.

Roberts, C., and H. Maillot, Paleoenvironments in the Weddell Sea area and Antarctic climates, as deduced from clay mineral associations and geochemical data, *Proc. Ocean Drill. Program, Sci. Results, 113*, 51-66, 1990.

Roeske, C. A., and M. H. O'Leary, Carbon isotope effect in the enzyme-catalyzed carboxylation of ribulose biphosphate, *Biochemistry, 23*, 6275-6285, 1984.

Romanek, C. S., E. L. Grossman, and J. W. Morse, Carbon isotopic fractionation in synthetic aragonite and calcite: Effects of temperature and precipitation, *Geochim. Cosmochim. Acta, 56*, 419-430, 1992.

Sage, R. F., Was low atmospheric CO_2 during the Pleistocene a limiting factor for the origin of agriculture?, *Global Change Biol., 1*, 93-106, 1995.

Savin, S. M., The history of the Earth's surface temperature during the past 100 million years, *Annu. Rev. Earth Planet. Sci, 5*, 319-355, 1977.

Savin, S. M., R. G. Douglas, and F. G. Stehli, Tertiary marine paleotemperatures, *Geol. Soc. Am. Bull., 86*, 1499-1510, 1975.

Savin, S. M., L. Abel, E. Barrera, D. Hodell, J. P. Kennett, M. Murphy, G. Keller, J. Killingley, and E. Vincent, The evolution of Miocene surface and near-surface marine temperatures: Oxygen isotopic evidence, in *The Miocene Ocean: Paleoceanography and Biogeography*, edited by J. P. Kennett, *Geol. Soc. Am. Mem., 163*, 49-82, 1985.

Schnitker, D., North-east Atlantic Neogene benthic foraminiferal faunas: tracers of deep-water palaeoceanography, in *North Atlantic Palaeoceanography*, edited by C. P. Summerhayes and N. J. Shackleton, *Geol. Soc. Spec. Publ., 21*, 191-203, 1986.

Schrag, D. P., D. J. DePaolo and F. M. Richter, Oxygen isotope exchange in a two-layer model of oceanic crust, *Earth Planet. Sci. Lett., 111*, 305-317, 1992.

Shackleton, N. J., The Carbon isotope record of the Cenozoic: History of organic carbon burial and

of oxygen in the ocean and atmosphere, in *Marine Petroleum Source Rocks*, edited by J. Brooks and A. J. Fleet, *Geol. Soc. Spec. Publ., 26*, 423-434, 1987.

Shackleton, N. J., and J. P. Kennett, Paleotemperature history of the Cenozoic and the initiation of Antarctic glaciation: Oxygen and carbon isotope analyses in DSDP sites 277, 279, and 281, *Initial Rep. Deep Sea Drill. Proj., 29*, 743-755, 1975.

Sharkey, T. D., and J. A. Berry, Carbon isotope fractionation of algae as influenced by an inducible CO2 concentration mechanism., in *Inorganic Carbon Uptake by Aquatic Photosynthetic Organisms*, edited by W. J. Lucas, and J. A. Berry, 389-401, *Am. Soc. Plant Physiol.*, Rockville, 1985.

Shipboard Scientific Party, Site 730, *Proc. Ocean Drill. Program Initial Rep.*, 117,555-584, 1989.

Spaulding, S., Neogene nannofossil biostratigraphy of Sites 723 through 730, Oman continental margin, northwestern Arabian Sea, *Proc. Ocean Drill. Program Sci. Results*, 117, 5-36, 1991.

Spero, H. J., and M. J. DeNiro, The influence of symbiont photosynthesis on the d18O and d13C values of planktonic foraminiferal shell calcite, *Symbiosis*, 4, 213-228, 1987.

Spero, H. J., and D. W. Lea, Intraspecific stable isotope variability in the planktic foraminifera *Globigerinoides sacculifer*: Results from laboratory experiments, *Mar. Micropaleontol.*, 22, 221-234, 1993.

Thomas, E., Early to middle Miocene benthic foraminiferal faunas from DSDP sites 608 and 610, North Atlantic, in *North Atlantic Palaeoceanography*, edited by C. P. Summerhayes and N. J. Shackleton, *Geol. Soc. Spec. Publ., 21*, 205-218, 1986.

Thunell, R., and P. Belyea, Neogene planktonic foraminiferal biogeography of the Atlantic Ocean, *Micropaleontology*, 28, 381-398, 1982.

Tsuzuki, M., and S. Miyachi, The function of carbonic anhydrase in aquatic photosynthesis, *Aquat. Bot.*, 34, 85-104, 1989.

Vincent, E., and W. H. Berger, Carbon dioxide and polar cooling in the Miocene: The Monterey hypothesis, in *The Carbon Cycle and Atmospheric CO_2: Natural Variations From Archean to Present, Geophys. Monogr. Ser., vol. 32*, edited by E. T. Sundquist and W. S. Broecker, AGU, Washington, D.C., 455-468, 1985.

Volkman, J. K., G. Eglinton, E. D. Corner, and J. R. Sargent, Novel unsaturated straight-chain C37-C39 methyl and ethyl ketones in marine sediments and a coccolithophore *Emiliania huxleyi*, in *Advances in Organic Geochemistry 1979: Proceedings of the Ninth International Meeting on Organic Geochemistry*, edited by A. G. Douglas and J. R. Maxwell, 219-227, Pergamon, Tarrytown, N.Y., 1980.

Weiss, R. F., Carbon dioxide in water and seawater: The solubility of a non-ideal gas, *Mar. Chem., 2*, 203-215, 1974.

Westerberg-Smith, M. J., Radiolarians for the North Atlantic Ocean, Deep Sea Drilling Project Leg 94, *Initial Rep. Deep Sea Drill. Proj., 94*, 763-778, 1987.

Wong, W. W., and W. M. Sackett, Fractionation of stable carbon isotopes by marine phytoplankton, *Geochim. Cosmochim. Acta, 42*, 1809-1815, 1978.

Woodruff, F., and S. M. Savin, Miocene deepwater oceanography, *Paleoceanography, 4*, 87-140, 1989.

Woodruff, F., and S. M. Savin, Mid-Miocene isotope stratigraphy in the deep sea: high-resolution correlations, paleoclimatic cycles, and sediment preservation, *Paleoceanography, 6*, 755-806, 1991.

Wright, J. D., and K. G. Miller, Control of North Atlantic deep water circulation by the Greenland-Scotland ridge, *Paleoceanography, 11*, 157-170, 1996.

Wright, J. D., K. G. Miller, and R. G. Fairbanks, Evolution of modern deepwater circulation: Evidence from the late Miocene southern oceans, *Paleoceanography, 6*, 275-290, 1991.

Wright, J. D., K. G. Miller, and R. G. Fairbanks, Early and middle Miocene stable isotopes: Implications for deepwater circulation and climate, *Paleoceanography, 7*, 357-389, 1992.

Zachos, J., J. Breza, and S. W. Wise, Early Oligocene ice-sheet expansion on Antarctic: Sedimentological and isotopic evidence from Kerguelen Plateau, *Geology, 20*, 569-573, 1992.

Zachos, J. C., K. C. Lohmann, J. C. G. Walker, and S. W. Wise, Abrupt climate change and transient climates during the Paleogene: A marine perspective, *J. Geol., 101*, 191-213, 1993.

Zachos, J. C., T. M. Quinn, and K. A. Salamy, High-resolution (10^4 years) deep-sea foraminiferal stable isotope records of the Eocene-Oligocene climate transition, *Paleoceanography, 11*, 251-266, 1996.

Zachos, J. C., B. P. Flower and H. Paul, Orbitally paced climate oscillations across the Oligocene/Miocene boundary, *Nature, 388*, 567-570, 1997.

M. A. Arthur and K. H. Freeman, Department of Geosciences, The Pennsylvania State University, University Park, PA 16872. (arthur@essc.psu.edu; kate@essc.psu.edu)

M. Pagani, Earth Sciences Department, University of California, Santa Cruz, CA 95064. (pagani@es.ucsc.edu)

(Received August 5, 1998;
revised December 29, 1998;
accepted January 22, 1999.)